Harvesting-induced evolution of collective behavior in a fish

Valerio Sbragaglia[a,1,2], **Pascal P. Klamser**[b,1], **Pawel Romanczuk**[b,3], **and Robert Arlinghaus**[a,c]

[a]Department of Biology and Ecology of Fishes, Leibniz-Institute of Freshwater Ecology and Inland Fisheries, Müggelseedamm 310, 12587 Berlin, Germany
[b]Department of Biology, Institute for Theoretical Biology, Humboldt-Universität zu Berlin, 10115 Berlin, Germany
[c]Division of Integrative Fisheries Management, Department of Crop and Animal Sciences, Faculty of Life Science, Humboldt-Universität zu Berlin, Invalidenstrasse 42, 10115 Berlin, Germany

Many fisheries around the globe preferentially capture large individuals with implications for the evolution of exploited populations. Fisheries-induced evolution may alter collective behavioral phenotypes through individual-level adaptations that affect boldness, swimming speed and tendency to follow social vs. environmental cues. Studying the behavioural mechanisms that give rise to possible changes in shoaling and other collective outputs is challenging in the wild, but first insights into whether intensive and size-selective harvesting could alter collective phenotypes and shoaling can be gathered through experiment of size-selective harvesting conducted in the laboratory. We present a multi-generation harvest selection experiment with zebrafish (*Danio rerio*) as a model species and demonstrate that large size-selective harvesting typical of global fisheries decreases risk-taking behavior of individuals, and surprisingly also decreases shoal cohesion. This counter-intuitive effect at the collective level is mechanistically caused by risk-averse individuals favored under large size-selective harvest paying more attention to environmental instead of social cues. Agent-based model simulations further reveal that fisheries-induced evolution of shoaling behavior is adaptive under fishing scenarios by decreasing exploitation rate. By contrast, the same collective behavior favored by size-selective harvesting is maladaptive in the presence of natural predation and increases natural mortality. The evolutionary adaptations we document may slowly, but steadily erode the natural fitness benefits offered by shoaling in many species targeted by global fisheries. Erosion of shoal cohesion can also negatively affect catchability with consequences for human well-being.

boldness | **cohesion** | **swimming** | **catchability** | **collective** | **fishing**

[1] V.S. and P.P.K. contributed equally to this work.

Correspondence:

[2]experimental data: valeriosbra@gmail.com

[3]models and simulations: pawel.romanczuk@hu-berlin.de

Contributions:

V.S. and R.A. designed the experiments; V.S. performed the experiments, the statistical test and analysed part of the experimental data. P.P.K. and P.R. developed the model. P.P.K. ran the simulations and analyzed part of the experimental data. V.S., P.P.K., P.R. and R.A. interpreted the data. V.S., P.P.K, P.R. and R.A. wrote the manuscript.

Introduction

Human harvesting of wild animals triggers unnatural selection in exploited populations (1, 2). Intensive and selective fishing can evolutionary alter life-history, physiological and behavioral traits (3–6), thereby affecting population dynamics (7, 8). Fisheries-induced evolution may also change carrying capacity, yield, reference points, catchability and recovery and is thus relevant from a fisheries-management perspective (9).

Catchability of individual fish is determined by morphological traits (e.g. body size), characteristics of the gear (e.g. mesh sizes), individual states (e.g. hunger) and individual behavioral traits (10). Although the relationship between individual behavioural traits and vulnerability to capture is increasingly documented (11, 12), there is limited knowledge about the prevalence of fisheries-induced evolution of behavior (1, 13) and how adaptive changes in individual behavioural traits affect collective phenotypes, such as shoaling. Collective behavior characterizes many fish species, including those of high relevance for global fisheries (e.g. small pelagics such as anchoveta, *Engraulis ringens*, and Atlantic herring, *Clupea harengus*). In fact, 13 out of the 25 most fished species in the world are strongly shoaling fish that account for about a quarter of total fisheries landings (14).

Fish shoaling behavior is a key driver of the capture process, e.g., in seining or trawling (15–17). Shoaling also has strong natural adaptive value by reducing predation risk and increasing foraging efficiency (18–20). The emergence of collective phenotypes in fish and other animals can be explained by simple interactions rules among individuals that are influenced by their respective neighbours (21, 22). Major group-level behavioural transitions can be triggered by minor changes in social interactions at the individual level (23). Therefore, fisheries-induced evolution might affect collective output such as shoaling by changing individual behavioral traits (e.g. boldness) that are involved in the interactions rules that drive group behavior (11).

Boldness (i.e. the propensity to take risks) is an individual behavioral trait that together with other traits, such as activity, sociability or aggression, determines catchability in fisheries (e.g. 11, 12). Individual-level behavioural traits such as boldness or swimming speed also play an important role in driving collective behavioral outputs such as shoal cohesion (e.g. 24). Large size-selective harvesting, where larger fish have a higher mortality risk than smaller ones, is a typical selectivity pattern in fisheries that has been shown to decrease individual boldness (3), and may in turn also affect collective phenotypes, such as shoaling.

Adaptive changes in individual fish boldness can emerge through at least three mechanisms (3, 9, 25). First, life histories and individual behavioral traits are often correlated following the pace of life (26). In turn, evolution of fast life histories typical in most fisheries (1, 9) is expected to favor

DRAFT

bold, aggressive and asocial fishes through correlated selection responses. Second, fisheries-induced changes in morphological traits, such as body size, can additionally bring about changes in individual behavioral traits because of systematic relationships of size and behavioural traits, such as boldness or activity (27). Finally, individual behavior traits can be under direct selection because they differentially expose fish to fishing gear (11, 12). Irrespective of the mechanism, fisheries-induced evolution of boldness or other individual behavioural traits (e.g., social proximity tendency; 28) can have important consequences for collective behaviours, such as shoal cohesion, which constitutes an insofar not tackled research question.

Experimental studies mimicking fisheries-induced evolution showed that female zebrafish *Danio rerio* exposed to small, but not to large, size-selective harvesting evolved low activity (a proxy of decreased swimming speed), spend less time in an open field (a proxy of decreased risk-taking behavior) and near conspecifics (a proxy of decreased sociability) compared to controls (29). These results were gathered from individual-level experimental trials. Preliminary studies using the same experimental system focusing at collective behavioral traits suggested unexpected outcomes of harvest selection. For example, shoals exposed to small size-selective harvesting took collectively more risks in the open field than control fish (29). This is the opposite response to the behavioural traits expressed by the fish when assayed individually, which took less risk compared to controls (29). Such results are also at odds with previous studies because individuals of social species that take less risk are expected to form more cohesive shoals (18, 19, 30–33). This is due to the selfish herd effect, which proposes that predation mortality risk decreases in more cohesive shoals (18), and the confusion effect, which assumes that attack rate of predators decreases with higher prey densities (33). Hence, a decrease of risk-taking behavior should be accompanied with an increase of shoal cohesion, but preliminary studies with the zebrafish selection lines suggested the opposite (34).

Related, a recent study in qingbo, *Spinibarbus sinensis*, showed that shoals composed of either exclusively shy or bold individuals were less cohesive than shoals formed by individuals with a diversity of boldness levels (24). Indeed the composition of the group in terms of individual behavioral traits affects collective behaviours (28, 35). Considering that the frequency of bold individuals is expected to systematically shift with fisheries-induced evolution (11), important effects on collective behavioral outputs are likely, but currently neither empirically demonstrated nor mechanistically explained.

Several mechanisms could shape how fisheries-induced evolution of individual phenotypes may affect collective behavior. For example, qingbo shoals with exclusively low active individuals (i.e. fish with slow swimming speed) formed more cohesive groups than shoals with heterogeneous activity levels (24). A correlation between slow swimming speed and shoal cohesion has also been demonstrated in stickleback, *Gasterosteus aculeatus* (28) and golden shiner, *Notemigonus crysoleucas* (36). In addition to individual behavioral phenotypes (e.g. boldness) and swimming speed, shoal cohesion may also be affected by a trade-off in the use of social vs. environmental cues to update behaviors within a shoal. For example, shoals predominantly composed by risk-averse fish – an adaption predicted in fisheries-induced evolution under large size-selective harvesting (3, 11) - might update their behavior by paying more attention to environmental cues in search for possible threats at the expense of paying less attention to their conspecifics, in turn reducing shoal cohesion. Our work examines whether such mechanisms could be at play in affecting changes in collective phenotypes from changes in individual-level behavioural traits in intensively exploited fish stocks.

Mechanistically, the swimming behavior of many fish can be characterized by the tail beat frequency (37), which allows to split the trajectories in burst phases (i.e., speed increases) followed by coast phases (38). Zebrafish exhibit a burst-coast-type swimming behavior that can be quantified from tracking data (38). Different burst rates lead to differences in group cohesion and speed (39). However, previous burst-coast models considered only social cues (38, 39), neglecting the importance of environmental cues possibly triggering burst responses of individual fish in a group. A full characterization of the individual-level mechanisms governing collective behavior should take into account all possible processes affecting individual behavior (in particular those related to risk perception) and the resulting movement decisions at the group level. In this context, exploring systematic variation in individual perception of, and response to, environmental cues as opposed to just social cues, is essential for developing a holistic understanding of how changes in individual risk perception may affect collective behavior under size-selective mortality selection from a mechanistic perspective.

We take advantage of a long-term harvesting experiment of zebrafish as a model shoaling species. Experimental populations were subjected to five generations of size-selective harvesting mimicking the fishing mortality scenario to be expected by intensive capture fisheries (6). The zebrafish lines that we studied were subjected to two treatments together with a control: large-harvested line (largest individuals preferentially harvested, the typical case in most fisheries), small-harvested line (smallest individuals preferentially harvested, a possible case in fisheries managed with a maximum-size limit or where dome-shaped selectivity is prevalent) and random-harvested line (control; individuals randomly harvested with respect to size). Previous results revealed substantial changes in life history, size variation, gene expression, allele frequencies as well as individual and collective behavioral traits (6, 29, 34, 40–42), but the mechanistic underpinning of the collective behavioral changes observed in the cited studies remained untackled.

We firstly characterized risk-taking and cohesion of the shoals to confirm previously documented preliminary patterns at the collective level (34). To fully understand the mechanistic process driving the resulting collective phenomena, we developed an individual-based model that related

DRAFT

individual-level traits (e.g., swimming speed and behavioral update using environmental vs. social cues) to group-level emergent properties. To that end, we used high resolution tracking to measure the swimming speed and the behavioral update rate of individual fish within groups to calibrate a burst-coast-agent-based model designed to study the individual mechanisms underlying the possible differences in shoal cohesion. Lastly, we used the model to simulate the collective behavior of the selection lines in the presence of a natural predator or fishing gear to build a reasoned hypothesis about the adaptive or possible maladaptive outcomes of fisheries-induced evolution of collective behavior in natural and human-shaped eco-evolutionary contexts.

Results

A. Risk-taking and shoaling behavior in groups. We characterized zebrafish behavior during feeding in a diving test where the time spent at the surface was interpreted as risk-taking behavior (see methods for details). Risk-taking behavior during feeding was significantly ($\chi^2_{(2)} = 15.059$; $p < 0.001$) different among selection lines. Specifically, the large- and small-harvested lines showed a lower and higher propensity to take risk than controls, respectively (Fig. 1A). When examining shoaling behavior in a round arena (see methods for details), we additionally found a significant effect of the selection lines on both mean inter-individual distance ($\chi^2_{(2)} = 9.553$; $p < 0.01$; inset in Fig. 1B) and mean nearest-neighbor distance ($\chi^2_{(2)} = 8.818$; $p < 0.05$; Fig. 1B). The large- and small-harvested lines formed less and more cohesive shoals than controls, respectively (Fig. 1B); the same pattern was observed for the nearest-neighbor distance (Fig. 1B). Note that the inter-individual distance showed the same trend as the nearest-neighbor distance, which means that the change in inter-individual distance was not related to a split of the main group into multiple subgroups.

B. Individual behavior in the shoal. We individually tracked fish behavior during shoaling (see methods for more details). Individual swimming speed was significantly ($\chi^2_{(2)} = 47.839$; $p < 0.001$) different among selection lines. Specifically, the small-, but not the large-harvested line, showed a slower swimming speed than controls (inset in Fig. 1C). Furthermore, the burst rate during collective movement was significantly ($\chi^2_{(2)} = 44.573$; $p < 0.001$) different among selection lines. Again the small-, but not the large-harvested line, bursted less frequently than controls (Fig. 1C). Note that the burst rate showed the same trend as the swimming speed, which suggests that differences in burst rate was the main cause of variation in swimming speed.

As expected and confirming previous studies with the same selection lines, the body size at age of the experimental fish varied significantly among the selection lines ($\chi^2_{(2)} = 32.862$; $p < 0.001$). The large-harvested line evolved smaller body length, while the small-harvested line expressed a larger body length than controls (Fig. 1D). This confirms a fixed evolutionary change in body length and hence growth rate in

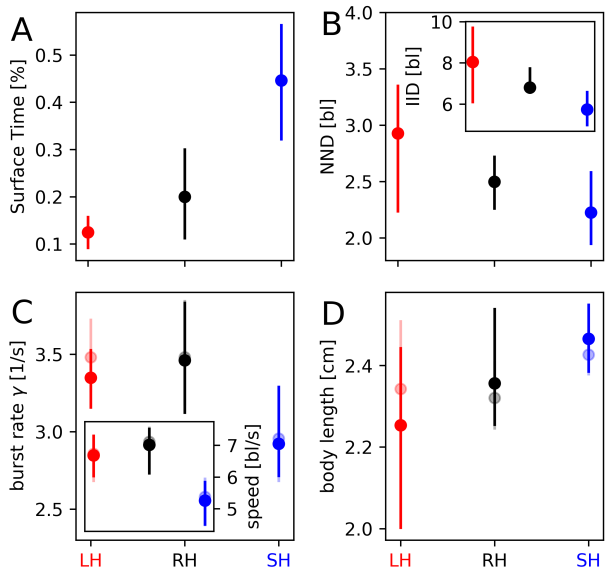

Fig. 1. Group level results for time spent feeding at the surface of the water during a diving test (A), mean group nearest-neighbor distance (expressed in body length; B) and inter-individual distance (expressed in body length; inset B). Individual level results for burst rate (C), speed (expressed in body length per second; inset C) and body size (D). The selection lines are indicated by different color (red=LH: large-harvested; black=RH: random-harvested; blue=SH: small-harvested). Bold colors (C , D) refers to the entire data set (N = 48), while shadowed colors refers to the subsample of size-matched individuals (N = LH: 24; RH: 36; SH: 40). Points represent the median and vertical lines represent the first (25th percentile) and third (75th percentile) quartiles.

response to size-selective harvest at F13 that is eight generations after the experimental harvest stopped (34). To control possible confounding effects of body size on the evolutionary effect of size-selective harvesting on behavior (see methods for more details) we composed a subsample of the dataset with size-matched individuals without significant ($\chi^2_{(2)} = 1.320$; $p = 0.517$) differences in body length among the lines (Fig. 1D). The above mentioned differences in speed and burst rate among the selection lines were still significant (speed: $\chi^2_{(2)} = 33.054$; $p < 0.001$; burst rate: $\chi^2_{(2)} = 34.457$; $p < 0.001$; Fig. 1C) when the subsample of size-matched individuals was used in the analyses. Moreover, body size did not relate to swimming speed ($\chi^2_{(2)} = 0.416$; $p = 0.519$) and burst rate ($\chi^2_{(2)} = 0.032$; $p = 0.858$).

C. Mechanistically linking micro-level interactions among individuals with macro-level collective outcomes. We showed a decrease in collective risk-taking behavior and a counter-intuitive increase in inter-individual distance in the large-harvested line, while the opposite was observed for the small-harvested line relative to the controls. To unravel the mechanistic underpinning of these results, we implemented a burst-coast-agent-based model. The most important aspect of the model, is that each individual burst event (Fig. 2A) represents either a response to a social cue (with probability P_{soc}) or to a random environmental cue (with probability $P_{env} = 1 - P_{soc}$). The probability P_{soc} was calibrated matching the experimental values related to nearest-neighbour distance (Fig. 1B) and individual swimming speed

DRAFT

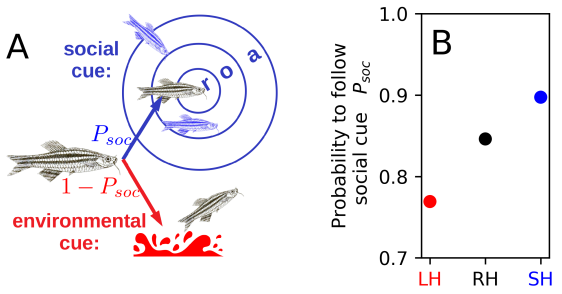

Fig. 2. (A) Schematic model description showing that at each burst an individual can follow with probability P_{soc} social cues (i.e. behaves according to a three-zone model: r=repulsion-, o=orientation-, a=attraction-zone) or with probability $1 - P_{soc}$ environmental cues. (B) Optimization results for fitting the burst-coast model to experimental data related to the probability to follow social cues P_{soc}. The selection lines differed, next to P_{soc} in their specific burst rate γ that was estimated from experimental data. The selection lines are indicated by different color (red=LH: large-harvested; black=RH: random-harvested; blue=SH: small-harvested). No error bars exist for the optimization. See methods for the robustness of the optimization results.

(inset in Fig. 1C) for each selection line. The burst rate γ was also set according to empirical data shown in Figure 1C). We assumed the remaining model parameters to be identical between the different selection lines, in line with empirical data (Tab. S1, S2). The calibration of the burst-coast model suggested that our experimental measures were best reproduced by the model if the large-harvested line had a higher tendency to follow environmental cues, and therefore followed social cues less often than the controls (Fig. 2B). The opposite was documented for the small-harvested line (Fig. 2B). We thus conclude that in addition to differences in burst rate also the tendency to follow social vs. environmental cues provide a mechanistic explanation for the observed differences in average individual swimming speed and emergent collective behavior among the selection lines.

D. Adaptive value of altered collective behaviour. We finally used the above-derived agent-based model representations of the three different selection lines to investigate whether the size-selective harvesting could have an impact on the ability of the shoals to evade a natural predator and different fishing gear (see methods and SI for details). The mean exploitation rate (i.e. number of fish killed per time) was computed in three different scenarios: (i) natural predation, including the possibility of a confusion effect (33), by a single mobile predator following the closest shoaling fish (Fig. 3A); (ii) fishing by a single agent without information about the position of the shoal (random search, similar to Fig. 3A; e.g., a fisher on a boat without an echo sounder); (iii) fishing by multiple aligned agents moving on a straight line towards the center of mass of the shoal (Fig. 3B; e.g., commercial trawling informed on the position of the shoal). Passive (e.g., a trap or hook-and-line sets) and active (e.g., seining or trawling) fishing gears were simulated by varying the speed of the fishing agents in the simulated scenarios. Fishing agents were able to capture a fish if it was closer than $r_{capture}$ thereby creating an encounter-based capture mechanism typical of many fisheries (43, 44), while the natural predator's capture was also influenced by the number of shoaling fish in its vicinity (i.e. confusion effect, see methods).

The natural predator (Fig. 3C) exploited the large-harvested line faster than the controls; while the opposite was observed for the small-harvested line (Fig. 3C). By contrast in all fishing scenarios (Fig. 3D, E), the fishing agents exploited the large-harvested line at a slower (i.e., less efficient) rate than the controls, and again the opposite was observed for the small-harvested line (Fig. 3D, E). Results are shown as relative standardized exploitation rate with respect to the controls (non-standardized values are shown in Figure S5). The difference between natural predation and the fishing scenarios vanished when the confusion effect was disabled in the model (Fig. S9) indicating that the differences in group cohesion among the selection lines caused the opposing patterns in avoiding natural predator and fishing agents. Note that the same results were obtained if the distance between fish and fishers/predator was used as alternative measure to the exploitation rate (Figs. S11F,G; S12F,G). To summarize, the simulations results suggested that the collective behavioural traits of the large-harvested line may increase survival in a fisheries context, but at the same time may increase mortality in a natural predation context, while the opposite was observed for the small-harvested line.

Discussion

Recent theoretical and conceptual studies have suggested that intensive harvesting may leave a strong legacy in the behaviour of exploited stocks (3, 11). Our experimental results agree with them. In particular the "timidity-syndrome hypothesis" proposes that intensive fishing reduces individual risk-taking behavior thereby reducing vulnerability to fishing gear, supporting the idea that size-selective harvest may bring about evolutionary changes in behavioural traits. (11). Using an experiment of size-selective harvesting we confirmed that changes in individual risk-taking behavior took place, which in turn shaped shoal cohesion. Classic theory related to group living animals predict that a reduction of individual risk-taking behavior – and hence an increase of risk-aversion - should result in individuals forming more cohesive shoals to reduce their probability of predation mortality (18). Our results challenge this prediction and we propose a mechanism explaining this counter-intuitive outcome. Specifically, by decreasing their risk-taking behavior (i.e. by being more risk averse), individuals in the large-harvested line payed more attention to possibly threatening environmental cues, which in turn affected their burst-and-coast movement behavior, thereby reducing shoal cohesion. Importantly, we demonstrated the exactly opposite adaptation in the small-harvested line, thereby showcasing that our results represented clean experimental outcomes that can be directly linked to the impact of size-selective harvest.

The risk-taking and shoaling behavioral adaptations we documented can be explained in two different ways. The first is related to an individual growth process mediated by foraging in risky contexts. During the selection (F1 – F5) zebrafish were fed with clumped food at the surface of the water (6). In their

DRAFT

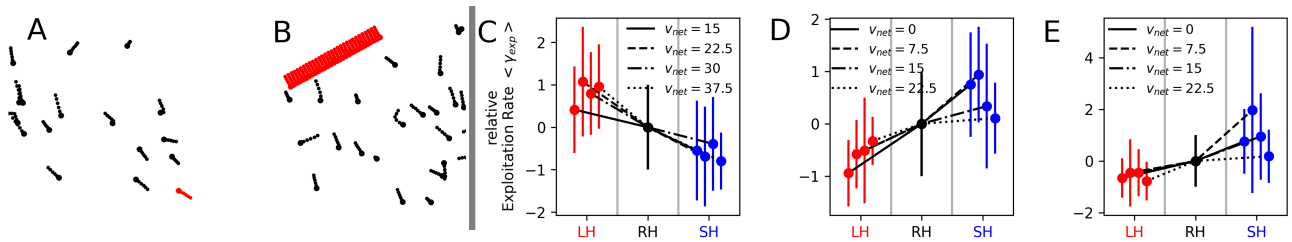

Fig. 3. Results of the natural predator scenario (A, C), the single fishing agent (A, D) and the multiple fishing agent scenario (B, E). $N = 30$ shoaling fish were simulated in a box of size $L = 100\ cm$ with periodic boundary conditions and swimming with a speed of $\langle v \rangle \approx 15\ cm/s$. The predator moved with $v_{net} = [15,\ 22.5,\ ,30,\ 37.5]\ cm/s$ while the fishing agents with $v_{net} = [0,\ 7.5,\ 15,\ 22.5]\ cm/s$ indicated by solid, dashed, dash-dotted and dotted line, respectively. Exploitation rates were reduced by the mean and divided by the standard deviation of the random-harvested line to standardize their values. Snapshots of a typical simulation are shown for the predator- and single-fishing-agent scenario (A) and for the multiple-fishing-agents scenario (B); the shoaling fish are represented in black and the predator and fishing agents in red. The relative mean exploitation rate $\langle \gamma_{exp} \rangle$ of the three selection lines (red=LH: large-harvested; black=RH: random-harvested; blue=SH: small-harvested) was shown for each of the simulated scenarios: predator (C), single fishing agent (D), and multiple fishing agents (E). The error bars indicated the standard deviation relative to the control line (RH) using a sample of 40 simulations.

natural environment the surface is a particularly risky environment for zebrafish due to the presence of avian predators (45). Zebrafish reduce the use of water surface in the presence of natural predation risk (46). Therefore, the large size-selective harvest removed those individuals that took more risk by foraging at the surface and hence grew more rapidly, favoring the evolution of less risk-taking behavior with respect to the controls. The opposite was documented for the small-harvested line, which was found to be bolder and faster growing. The second explanation is related to a direct selection of individual sociability. Zebrafish attain a higher food consumption rate when they are in small groups than alone (47). Therefore, the large size-selective harvest should have removed those individuals that fed in small groups because it should have provided individual fish advantages in accessing food, thereby favoring more solitary individuals and thus reducing shoal cohesion. However, when assaying individual sociability the large-harvested line was not found to differ from controls (29). Thus, it is unlikely that direct selection on individual sociability is an explanation for the reduced shoal cohesion reported here.

The burst-coast-agent-based model linked risk-taking of individuals with shoal cohesion and further helped explaining the harvesting-induced changes in collective phenotypes by assuming the existence of a trade-off between social and environmental information in collective motion (48). Our model is similar to previous work in terms of splitting the movement of shoaling fish into an active and passive phase (38, 39, 49). However, it provides a novel perspective on collective movements of fish shoals by linking risk perception and movement decisions. In fact, most previous models of collective behavior only account for social information (23, 39, 49–51), while our model explicitly considers how the motion of shoaling fish is influenced by the trade-off between random environmental and social cues. Previous simulation studies considered similar mechanisms (e.g., when moving agents directly react to a non-conspecific cue as a predator (32, 52) or a food-patch (53)); however, the moving agents were able to access non-conspecific information without costs alongside the social information. In our model, the tendency to follow/weight environmental cues limits the capacity to react to social cues and thus affects the individual behavior even in the absence of environmental cues. Another major difference to most existing models (23, 28, 51) is that the individual speed is not a model parameter but emerges from the interplay of burst rate, strength, duration and the tendency to follow social cues. Especially the dependency on the tendency to follow social cues makes it, to our best knowledge, unique. Our work suggest a link between individual risk-taking behavior and the increased attention to environmental cues on a mechanistic level because both speed and social responsiveness were emergent properties of shoaling fish interacting with their social and non-social environment. Note that our approach is conceptually different and goes beyond the association between speed and sociability (28). Instead, we introduced a mechanism that provides an explanation for the observed counter-intuitive results discussed above and, at the same time, reproduced the fundamental correlation between speed and social responsiveness (28).

The simulations of natural predation and fishing harvesting revealed that the collective behavioral adaptations of the large-harvested line are likely maladaptive under natural predation, but are adaptive in a fishing context (and vice versa for the small-harvested line). Specifically, in our model the decrease of shoal cohesion of the large-harvested line decreased vulnerability of shoals under a multitude of simulated fishing scenarios considering passive and active gear as well as single and multiple fishing agents. Fisheries-induced evolution of maladaptive behavior under natural contexts has been previously reported but only for individual behavioral traits and for changes in life-history traits such as maturation size (54). We moved a step forward providing evidence of possible maladaptive outcomes of collective behavioral traits (i.e. shoal cohesion) that have strong fitness value in many shoaling teleosts when attempting to reduce risk of natural predation (20). Our study suggests that intensive fishing mortality directed at the largest individuals of a population could shift the fitness optimum of shoaling behavior in the opposite direction of what natural selection would favor. Adaptive evolution under anthropogenic selection has been demonstrated to occur within few generations (1, 4, 6, 55–57), and could impede recovery of exploited population even after harvest-

DRAFT

ing halted (7). Our study provides the first functional integration of individual behavior into mechanisms governing group dynamics in the context of fishing exploitation. Moreover, our work proposes a new mechanism that could increase the natural mortality associated with fisheries-induced evolution and thereby negatively affect recovery, even if harvesting halted.

Previous studies have shown that fisheries-induced evolution of life histories can substantially increase natural mortality (58, 59). Elevated and size-selective harvesting triggers the evolution of a fast life-history, characterized by early maturation and small size, elevated reproductive investment and reduced post-maturation growth (60). Natural mortality decreases with length in fishes (61); therefore a decrease in body size is linked to an increase of natural mortality. In addition, an increase of reproductive investment is associated to an increase of natural mortality due to the cost of spawning (58, 62). Moreover, elevated and unselective fishing mortality is expected to increase boldness and in turn increase natural mortality through risk-taking behavior (58). In our study we focused on the latter aspect, but our results indicated that elevated mortality in combination with large size-selective harvest decreased boldness in agreement with theoretical work where large individuals are selectively harvested (3). Yet, while decreased boldness might reduce natural mortality, we propose that the decrease of shoal cohesion emerging from the evolution of increased individual risk-taking behavior can be a further mechanism by which natural mortality increases in a fisheries-induced evolution context where large individuals are preferentially harvested. We therefore extended the framework presented by Jørgensen and Holt (58) for unselective fisheries harvest revealing an insofar unknown mechanism by which fisheries-induced evolution of individual behavioral trait (e.g. boldness) through size-selection may drive collective outcomes that may be maladaptive under natural predation and elevate mortality in shoaling fishes.

Our predictions related to an increase of natural mortality in global fisheries scenarios associated with fisheries-induced evolution of shoaling are based on model simulations and future empirical research is needed to confirm our predictions. Therefore, the direct translation of our findings to real fishing scenarios should be done with great care. The absence of predatory pressure during our experimental evolution removed a selection pressure that could favor the increase of group cohesion despite the presence of size-selective fisheries. Also, the behavioural phenotypes assayed in the present study were measured under controlled conditions in the absence of natural predators. These simplifications should be carefully addressed in future studies. Before this research becomes available, anecdotal evidence from fishers of small pelagic species in the North-Western Mediterranean Sea (M. Coll, personal communication) and Norway (K. Enberg, personal communication) suggested that shoaling behavior and in particular cohesion of small pelagic species is decreasing with negative effects on catchability. In particular Mediterranean fishers associate such behavioral changes to the increase of predation pressure by recovering top predators such as bluefin tuna (*Thunnus thynnus*), but the mechanisms we describe here could be simultaneously at play. Our predictions could be important in a global context where populations of top predators are recovering and the increase of predation rate could impede stock rebuilding and even drive some species to extinction (e.g. 63). If, however, the experimental results we present hold in the wild, our study has important implications for global fisheries because selective harvesting of large individuals may affect catchability, recovery and contribute to fisheries-induced evolutionary "suicide" over contemporary time-scales in many shoaling species that happen to form the bulk of global fisheries.

Material and Methods

A. Selection lines. Our study system consisted of wild-collected zebrafish from West Bengal in India (for more details see 42, 64). The parental wild-collected population was experimentally harvested over five generations by exposing them to strong directional selection (a 75 percent per-generation harvest rate) for either small body size (large-harvested line) or large body size (small-harvested line). A third line was harvested randomly with respect to size and use as a control (random-harvested line). Each selection line was replicated twice for a total of six lines. Size-selective harvesting was applied during the first five generations (6) and then harvesting was stopped for eight further generations until F13 – a time when the present experimental trials took place. At F9 the large-harvested line evolved a smaller adult length and weight and higher relative fecundity compared to controls (6). By contrast, the small-harvested line showed reduced reproductive investment and no change in adult length compared to the control line (6). Both size-selected lines evolved different maturation schedules by maturing smaller and at younger age than the control line (for more details see 6). These differences persisted until F13 as shown elsewhere (29). Overall, the size-selection triggered changes in energy allocation patterns, with the large-harvested line investing early and intensively into reproduction, and the small-harvested line investing early but at low intensity into gonad production and more intensively in somatic growth. Moreover, the selection lines differed significantly in their behavioural traits, size variability, allele frequency and gene expression profiles (6, 29, 34, 40–42)

B. Experimental design. We stocked 8 juvenile zebrafish at 30 days post fertilization from each of the six selection lines into three-liter rearing boxes. All the boxes were housed on the shelves of the same holding system with a randomized order (5 replicates for each line; N = 10 for each line treatment). Throughout the experiment zebrafish were fed ad libitum with dry food (TetraMin, Tetra), the water temperature was maintained at 26±0.5 °C and photoperiod at 12:12 h light-darkness cycle (light on/off at 07:00 and 19:00, respectively). We run the experimental trials described below when zebrafish were 190-230 days post fertilization. All trials were run between 09:00 and 14:00. We started the experimental trials two hours after light-on to avoid measuring mating behavior that usually occurs in the first hours after light-on (65). The movement of the fish from the rearing boxes to the experimental tanks was conducted by gently pouring them together with the water from the stocking box. The experimental protocols were approved by the Spanish National Committee and the Committee of the University of Murcia on Ethics and Animal Welfare (CEEA-OH 491/2019).

C. Risk-taking experiment. Risk-taking behavior was measured in groups of 8 zebrafish moving them from the three-liter rearing boxes to a new experimental tank (width x length x height = 10 x 30 x 25 cm) with about 21 cm of water and conducting a diving test. A similar test has been repeatedly used to characterize behavioral phenotypes in zebrafish and is known to robustly measure risk-taking in this species (66). The experimental tank was placed on a table behind a white curtain to minimize disturbance to the fish during the experimental trials. On the side of the experimental tank (at about 50 cm) we placed a webcam (resolution: 1920 x 1080 pixels; frame rate: 30 frames per second) that was connected to a computer where video recordings were stored. Zebrafish were introduced in the experimental tank and left undisturbed for 3 min before starting the experimental trial. That time was sufficient to remove the diving response usually seen (66). Then,

DRAFT

a small quantity of food was added and at the same time we started video recording for 30 s (sufficient time for zebrafish to consume almost all the food) to quantify the time the individuals spent at the surface.

D. Shoaling experiment. Shoaling behavior in groups of 8 zebrafish was measured in a white round arena (diameter of 60 cm) with 10 cm of water. The arena was placed on a table behind a white curtain to minimize disturbance to the fish during the experimental trials. On top of the arena (at about 1 m) we placed a webcam (resolution: 1920 x 1080 pixels; frame rate: 30 frames per second) that was connected to a computer where video recordings were stored. Zebrafish were introduced in the experimental arena and left undisturbed for 25 min before starting the experimental trial. Video recording lasted 5 min and after that we measured the standard length of each fish on a petri dish with millimeter paper anesthetizing the fish using a clove oil dilution in ethanol and water.

E. Behavioral tracking. The video recordings related to risk-taking behavior were analyzed with automated behavioral tracking (EthoVision XT 9, Noldus Information Technologies Inc.; www.noldus.com). We calculated the cumulative time each of the 8 fish spent feeding at the surface of the experimental tank (one third of the water column = at about 7 cm). We considered this phenotype as a risky behavior because a reduced used of water surface has been documented in the presence of predation risk in this species (46). The video recordings related to shoaling were analyzed with the idTracker software. The software extracts specific characteristics of each individual and uses them to identify each fish without tagging throughout the video. This method avoids error propagation and is able to fully solve crossing, superposition of animals and occlusion problems (67).

F. Data analysis. We calculated group-level variables for shoaling behavior such as inter-individual distance (i.e., the average distance of a given fish from all the other fish in the arena) and nearest-neighbor distance (i.e., the nearest distance of a given fish from one of the other fish in the arena). We only considered the frames where all the shoal members were detected, and we used the mean body length of the group as a measure of both inter-individual and nearest-neighbor distances. We also calculated individual-level variables such as speed and burst rate. In this case, the output of the behavioral tracking was filtered by eliminating the coordinates of the individuals with a probability of correct identification lower than 0.85. The conservative filter reduced the number of trials used in the individual analysis (18 out of the 30 trials were used; N = 6 for each line treatment), but it increased the overall quality of the tracking output (on average of more than 90 percent of the fish identities were successfully solved). Our modelling approach focused on burst and coast phases, therefore individual identification was vital because properties of the burst phase, as its duration and rate, can be corrupted by tracking inaccuracy (Fig. S7). Assuming that the inaccuracy was random, we used a moving average with a Gaussian kernel to correct it. To estimate the standard deviation σ_{smoo} of the Gaussian kernel, we computed the number of burst events in a time interval of 2000 frames and compared it with a manually counted number. The closest approximation of burst events corresponded to $\sigma_{smoo} \approx 1.13$ (Fig. S8).

G. Statistical approach. Group measurements (risk-taking behavior, inter-individual distance and nearest-neighbor distance) and individual measurements (body size, speed and burst rate) were transformed when necessary by finding the exponent (λ), which made the values of the response variable as normally distributed as possible with a simple power transformation. Then, response variables were modelled using linear mixed effects models with selection lines as fixed effect and selection line replicate as random intercepts. Likelihood ratio tests were used to assess the significant effect of selection lines as fixed effect. Considering that zebrafish behavior is correlated with size (68) and that the size-selective treatments modified the size at age of the selection lines (6), it is conceivable that size differences among the selection lines could have masked evolutionary adaptations in terms of individual behavior. We thus estimated the effect of size (standard length) as a covariate against individual behavior to reveal whether selection treatment per se affected the evolution of behavior, or whether changes in the size of fish indirectly altered behavior in the evolved lines. As regards individual behaviors we implemented a second set of models with the size-matched dataset (Fig. 1D). The response variables were modelled by using linear mixed models and implementing all possible models (i.e., four) with individual body length as covariate, selection lines as fixed effect and selection line replicate as random intercepts. Likelihood ratio tests were used to assess the significant effect of selection lines and body length.

H. Shoaling model (burst and coast model). In the agent-based model of shoaling fish, the changes in position and velocity of fish i are described by the following equations of motion:

$$\frac{d\vec{r}_i}{dt} = \vec{v}_i\ , \quad \vec{v}_i = v_i(\cos\varphi_i, \sin\varphi_i)^T \tag{1}$$

$$\frac{dv_i}{dt} = -\beta v_i + \langle \vec{F}_i, \hat{e}_{v,i}\rangle, \quad \frac{d\varphi_i}{dt} = \frac{\alpha}{v}\langle \vec{F}_i, \hat{e}_{\varphi,i}\rangle \tag{2}$$

with β being the friction coefficient. v_i is the velocity of the focal agent along its heading direction, while φ_i is the polar angle defining the heading direction. $\langle \vec{F}_i, \hat{e}_{v,i}\rangle$ and $\langle \vec{F}_i, \hat{e}_{\varphi,i}\rangle$ are the projections of the burst force on the heading vector $\hat{e}_{v,i} = (\cos\varphi_i, \sin\varphi_i)$ and the perpendicular direction $\hat{e}_{\varphi,i} = (-\sin\varphi_i, \cos\varphi_i)$, respectively (69).

Fish accelerate only during the burst-phase, which corresponds to a non-zero force $\vec{F}_i$ during a burst:

$$\vec{F}_i(t) = \begin{cases} \vec{f}_{soc}(t) \text{ or } \vec{f}_{env}(t) & \text{during burst} \\ 0 & \text{during coast} \end{cases} \tag{3}$$

This bursting force models the response to either social or environmental cues. During the coast phase no force is applied and fish decelerate due to friction.

Due to the short burst duration ($t_b = 0.12\ s$) the heading may not equal the intended direction (i.e. the force direction). Additionally, experimental data suggests that turning starts prior to the acceleration in velocity direction (Fig. S7). Therefore we account for it by introducing a turning parameter $\alpha > 1$ in Eq. 2 that enhances the angular change. For a more detailed motivation and derivation see SI.

The burst behavior is defined by the burst rate γ, duration t_b and the burst force $\vec{F}_i$. The fish decides at the start of a burst with a probability P_{social} to react (socially) to the other fish or, with probability $1 - P_{social}$, to environmental cues. We assume that a fish should react to a threat stronger than to social cues (e.g. startle responses).

The social force $\vec{f}_{soc}$ is implemented according to the well established Couzin model (23). A fish reacts to conspecifics by turning away to avoid collisions at short distances $r < r_r$, by aligning at intermediate distances $r_r < r < r_o$, and by being attracted at large distances $r_o < r < r_a$ (Fig. 2A). The direction of the alignment force of fish i is the summation of the velocity differences $\vec{v}_{ji} = \vec{v}_j - \vec{v}_i$ to its nearest neighbors in the alignment zone. We assume interactions with the first shell of nearest neighbors (Voronoi neighbors). Corresponding interaction networks have been shown to approximate well visual interactions (70), and can be very efficiently computed in comparison to visual networks.

If neighbors of the focal fish occupy different zones simultaneously the following rules are applied. If at least one neighbor is in the repulsion zone the alignment and attraction neighbors are ignored. Otherwise, the direction of the social force is a weighted average of the alignment- and attraction-direction. The weights are the number of fish in the respective zone.

If the simulated predator/fishing agent is detected, then the environmental force $\vec{f}_{env}$ is given by a direct avoidance force (repulsion) away from it with a constant amplitude. If no existing threat is detected, the polar angle setting the burst direction due to environmental cues is drawn randomly from a uniform distribution $U(-\Pi, \Pi)$. The latter case is motivated by the fish misinterpreting non-controllable random perturbations (e.g. water reflections) as a threat and responding to them accordingly.

A predator or fishing agent p is detected by fish i with probability

$$P_{i,p,detect} = \frac{2}{1 + r_{pi}/r_f} \tag{4}$$

which equals one if $r_{pi} = |\vec{r}_p - \vec{r}_i| = r_f$. If $P_{detect} > 1$ it is set to 1. r_f is the detection distance which was for all simulations $r_f = 7\ cm$. This value is reasonable because fish should be able to detect a predator when they are likely to be captured $r_f \geq r_{capture} = 5\ cm$.

Additional parameters describing the repulsion force from the wall are avoided by a parameter free wall-avoidance mechanism ensuring that the fish avoids the wall while pursuing its intended direction (see SI for details).

DRAFT

I. Natural predator. The predator always moves directly to the closest simulated fish (Fig. 3A) with $v_{net} = 15,\ 22.5,\ 30,\ 37.5\ cm/s$ that is equal or larger compared to the speed of the simulated fish ($\langle v \rangle \approx 15\ cm/s$) because predators are usually larger than prey and therefore can swim faster (71, 72). In contrast to a fishing agent, most predators attack a specific fish and therefore need to focus on it before attacking. The so-called confusion effect (73), the disruption of the predator focus by a large number of individuals who are difficult to distinguish by phenotype and movement, is believed to be one key benefit of group living (19). We model the probability of a prey to be successfully captured if it is closer to the predator than $r_{capture} = 5cm$ within a small time window $[t, t+\delta t]$ as

$$p_{success,i}(t, \delta t) = p_{confuse}(t) \cdot \gamma_a \delta t \tag{5}$$

Here $\gamma_a = 1/s$ is a base predator attack rate (representing its handling time) and $p_{confuse}(t)$ represents the confusion effect that modulated the attack rate. The confusion term decreases $p_{success}$ with increasing number of perceived prey (33). A fish is sensed by a predator if it is closer than $r_{sense} = 4r_{capture}$. We assume a sigmoidal dependence on the number of sensed shoaling fish N_{sensed}:

$$p_{confuse} = 0.5 \tanh(-(N_{sensed} - N_{conf})) + 1 \tag{6}$$

Here $N_{conf} = 4$ is the number of sensed shoaling fish at which $p_{confuse} = 0.5$ (73). Thus, each shoaling fish has the same probability to be captured if it is closer to the predator than $r_{capture} = 5\ cm$.
Note that we repeated the natural predation simulation with a more realistic predator that is only able to attack one prey at a time and its capture success linearly depends on the distance to the prey. In agreement with the results of the main text, without the confusion effect the large-harvested line performed worse than control against natural predators (Fig. S9), while with confusion effect it performed better than controls (Fig. S10).

J. Fishing agents. The fishing agents are assumed to be stationary ($v_{net} = 0\ cm/s$), simulating passive gear or moving at a constant speed $v_{net} = 7.5,\ 15,\ 22.5\ cm/s$, thereby simulating active gear, while shoaling fish move with an average swimming speed ($\langle v \rangle \approx 15\ cm/s$). Fishing agents always capture a shoaling fish if it is closer than $r_{capture} = 5\ cm$.

Single fishing agent. In the single fishing agent scenario (Fig. 3A), the agent performs a random search with constant speed v_{net}. For different speed values the angular noise is adapted such that the persistence length is constant. The agent is either stationary (e.g. pots or trap fisheries) or moves randomly (e.g. angler on a boat without information about shoal location) with a fixed persistence length, i.e. its change in angle after travelling a certain distance is independent of its velocity. The angular change is given by

$$d\varphi/dt = \hat{\sigma}_\varphi \xi(t) \tag{7}$$

with $\xi(t)$ as Gaussian white noise. To account for the constant persistence length the noise level is speed dependent $\hat{\sigma}_\varphi = \sigma_\varphi \sqrt{v_{net}}$. See SI for a detailed derivation.

Multiple fishing agents. In the multiple aligned fishing agents scenario (Fig. 3B), the agents ($N_f = 20$; red) are aligned on a line spanning $L/4$ and they are either stationary (e.g. simulating gill nets or long lines) or moving perpendicular to their linear extension (e.g. simulating a trawling net). After travelling for a distance $L/2$, the fishing agent array is recreated at a distance of $L/4$ away from the center of mass of the shoal and restarts its movement in its direction.

K. Model parameter estimation. The estimated parameters of the model are summarized in Table S2. The forces f_{soc} and f_{env} can not be distinguished in the experiment. Therefore, only the burst acceleration F was measured instead. The estimation of the burst acceleration F and the burst duration t_b was done by splitting all data in burst and coast phases. Burst and coast phases were characterized by an increase and decrease of the speed of the shoaling fish, respectively. t_b was the mean length and F the mean acceleration of a burst period and they did not differ significantly between harvesting lines (see SI and Fig. S3). The burst rate γ was computed from a Gaussian moving mean over the binary time series of burst starts. The friction coefficient β was estimated by the deceleration during coast phases. The range of the different zones was difficult to estimate from empirical data, therefore we assumed that the repulsion range r_r corresponded roughly to fish body length (BL), and we estimated $r_r \approx BL/4 \approx 0.5\ cm$ because the ratio of length over width was about 5.

L. Model parameter optimization. To fit the model to the empirical data we applied the covariance matrix adaptation evolution strategy (74), from the Python package *pycma* (75). This optimizer is a good choice for multi-modal target functions ("fitness") without known gradients and a high-dimensional search space. We minimized the square-standardized differences between the simulated and experimentally observed values of the nearest-neighbor distances and the average individual speeds. The differences were standardized by their experimental standard deviation. All parameters were kept equal across the different selection lines apart from the burst rate γ, which was set to experimental values (Fig. 1C), and the tendency to socially update P_{soc}, which was optimized. The parameters alignment range (r_o), social- (f_{soc}), environmental force (f_{env}), friction (β) and turning coefficient (α) were fitted because they were difficult ($\beta,\ r_o$) or impossible ($f_{soc},\ f_{env},\ \alpha$) to estimate. The other parameters were set to values estimated in section F. All parameters are summarized in Table S2.

The covariance matrix adaptation evolution strategy results suggest that P_{soc} differed among the selection lines as $P_{soc}(large-harvested) < P_{soc}(random-harvested) < P_{soc}(small-harvested)$. The generality of this result was substantiated by a five-dimensional parameter scan. In the one percent of parameter configurations (≈ 169) with the smallest differences to experimental data (Fig. S6) 89 percent of the simulations agreed with the finding (see SI for details).

Bibliography

1. Mikko Heino, Beatriz Díaz Pauli, and Ulf Dieckmann. Fisheries-induced evolution. *Annual Review of Ecology, Evolution and Systematics*, 46(1):461–480, 2015. ISSN 1543-592X. doi: 10.1146/annurev-ecolsys-112414-054339.
2. Fred W. Allendorf and Jeffrey J. Hard. Human-induced evolution caused by unnatural selection through harvest of wild animals. *Proceedings of the National Academy of Sciences, USA*, 106(Supplement 1):9987–9994, 2009. doi: 10.1073/pnas.0901069106.
3. Ken H. Andersen, Lise Marty, and Robert Arlinghaus. Evolution of boldness and life history in response to selective harvesting. *Canadian Journal of Fisheries and Aquatic Sciences*, 75(2):271–281, 2018. ISSN 0706-652X 1205-7533. doi: 10.1139/cjfas-2016-0350.
4. David O. Conover and Stephan B. Munch. Sustaining fisheries yields over evolutionary time scales. *Science*, 297(5578):94–96, 2002. doi: 10.1126/science.1074085.
5. J. Hollins, D. Thambithurai, B. Koeck, A. Crespel, D. M. Bailey, S. J. Cooke, J. Lindstrom, K. J. Parsons, and S. S. Killen. A physiological perspective on fisheries-induced evolution. *Evolutionary Applications*, 11(5):561–576, 2018. ISSN 1752-4571 (Print) 1752-4571 (Linking). doi: 10.1111/eva.12597.
6. Silva Uusi-Heikkilä, Andrew R. Whiteley, Anna Kuparinen, Shuichi Matsumura, Paul A. Venturelli, Christian Wolter, Jon Slate, Craig R. Primmer, Thomas Meinelt, Shaun S. Killen, David Bierbach, Giovanni Polverino, Arne Ludwig, and Robert Arlinghaus. The evolutionary legacy of size-selective harvesting extends from genes to populations. *Evolutionary Applications*, 8(6):597–620, 2015. ISSN 1752-4571. doi: 10.1111/eva.12268.
7. Katja Enberg, Christian Jørgensen, Erin S. Dunlop, Mikko Heino, and Ulf Dieckmann. Implications of fisheries-induced evolution for stock rebuilding and recovery. *Evolutionary Applications*, 2(3):394–414, 2009. ISSN 1752-4571. doi: 10.1111/j.1752-4571.2009.00077.x.
8. Mikko Heino, Loc Baulier, David S. Boukal, Bruno Ernande, Fiona D. Johnston, Fabian M. Mollet, Heidi Pardoe, Nina O. Therkildsen, Silva Uusi-Heikkilä, Anssi Vainikka, Robert Arlinghaus, Dorothy J. Dankel, Erin S. Dunlop, Anne Maria Eikeset, Katja Enberg, Georg H. Engelhard, Christian Jørgensen, Ane T. Laugen, Shuichi Matsumura, Sébastien Nusslé, Davnah Urbach, Rebecca Whitlock, Adriaan D. Rijnsdorp, and Ulf Dieckmann. Can fisheries-induced evolution shift reference points for fisheries management? *ICES Journal of Marine Science*, 70(4):707–721, 2013. ISSN 1054-3139. doi: 10.1093/icesjms/fst077.
9. Christian Jørgensen, Katja Enberg, Erin S. Dunlop, Robert Arlinghaus, David S. Boukal, Keith Brander, Bruno Ernande, Anna G. Gårdmark, Fiona Johnston, Shuichi Matsumura, Heidi Pardoe, Kristina Raab, Alexandra Silva, Anssi Vainikka, Ulf Dieckmann, Mikko Heino, and Adriaan D. Rijnsdorp. Ecology: managing evolving fish stocks. *Science*, 318(5854):1247–1248, 2007.
10. Robert J. Lennox, Josep Alós, Robert Arlinghaus, Andrij Horodysky, Thomas Klefoth, Christopher T. Monk, and Steven J. Cooke. What makes fish vulnerable to capture by hooks? a conceptual framework and a review of key determinants. *Fish and Fisheries*, 18(5):986–1010, 2017. ISSN 1467-2979. doi: 10.1111/faf.12219.
11. Robert Arlinghaus, Kate L. Laskowski, Josep Alós, Thomas Klefoth, Christopher T. Monk, Shinnosuke Nakayama, and Arne Schröder. Passive gear-induced timidity syndrome in wild fish populations and its potential ecological and managerial implications. *Fish and Fisheries*, 18(2):360–373, 2017. ISSN 1467-2979. doi: 10.1111/faf.12176.
12. Beatriz Diaz Pauli and Andrew Sih. Behavioural responses to human-induced change: Why fishing should not be ignored. *Evolutionary Applications*, 10(3):231–240, 2017. ISSN 1752-4571. doi: 10.1111/eva.12456.
13. Silva Uusi-Heikkilä, Christian Wolter, Thomas Klefoth, and Robert Arlinghaus. A behavioral perspective on fishing-induced evolution. *Trends in Ecology Evolution*, 23(8):419–421, 2008. ISSN 0169-5347. doi: 10.1016/j.tree.2008.04.006.
14. FAO. *The state of world fisheries and aquaculture (SOFIA) - meeting the sustainable development goals. Food and Agriculture Organization, Rome, Italy, (p. xiii + 210)*. 2018.
15. Yoo-Won Lee, Tohru Mukai, Kohji Iida, Doo-Jin Hwang, and Hyeong-Il Shin. The application of image processing technology for the analysis of fish school behavior: Evaluation of fish school behavior response to the approaching vessel using scanning sonar. *Fisheries and Aquatic Sciences*, 5(3):212–218, 2002. ISSN 2234-1749.

DRAFT

16. Ole Arve Misund. Avoidance behaviour of herring (*Clupea harengus*) and mackerel (*Scomber scombrus*) in purse seine capture situations. *Fisheries Research*, 16(2):179–194, 1993. ISSN 0165-7836.
17. Maria Tenningen, Gavin J. Macaulay, Guillaume Rieucau, Héctor Peña, and Rolf J. Korneliussen. Behaviours of atlantic herring and mackerel in a purse-seine net, observed using multibeam sonar. *ICES Journal of Marine Science*, 74(1):359–368, 2016. ISSN 1054-3139. doi: 10.1093/icesjms/fsw159.
18. W. D. Hamilton. Geometry for the selfish herd. *Journal of Theoretical Biology*, 31(2):295–311, 1971. ISSN 0022-5193. doi: https://doi.org/10.1016/0022-5193(71)90189-5.
19. Jens Krause and Graeme D Ruxton. *Living in groups*. Oxford University Press, 2002. ISBN 0198508182.
20. TJ Pitcher, AE Magurran, and IJ Winfield. Fish in larger shoals find food faster. *Behavioral Ecology and Sociobiology*, 10(2):149–151, 1982. ISSN 0340-5443.
21. Iain D. Couzin and Jens Krause. *Self-Organization and Collective Behavior in Vertebrates*, volume 32, pages 1–75. Academic Press, 2003. ISBN 0065-3454. doi: https://doi.org/10.1016/S0065-3454(03)01001-5.
22. James E Herbert-Read, Andrea Perna, Richard P Mann, Timothy M Schaerf, David JT Sumpter, and Ashley JW Ward. Inferring the rules of interaction of shoaling fish. *Proceedings of the National Academy of Sciences, USA*, 108(46):18726–18731, 2011. ISSN 0027-8424.
23. Iain D Couzin, Jens Krause, Richard James, Graeme D Ruxton, and Nigel R Franks. Collective memory and spatial sorting in animal groups. *Journal Theoretical Biology*, 218(1): 1–11, 2002. ISSN 00225193. doi: 10.1006/yjtbi.3065.
24. Zhong-Hua Tang and Shi-Jian Fu. Qingbo (*Spinibarbus sinensis*) personalities and their effect on shoaling behavior. *Acta Ethologica*, 22(2):135–144, 2019. ISSN 0873-9749.
25. Marion Claireaux, Christian Jørgensen, and Katja Enberg. Evolutionary effects of fishing gear on foraging behavior and life-history traits. *Ecology and Evolution*, 8(22):10711–10721, 2018. ISSN 2045-7758 (Print) 2045-7758 (Linking). doi: 10.1002/ece3.4482.
26. Denis Réale, Dany Garant, Murray M. Humphries, Patrick Bergeron, Vincent Careau, and Pierre Olivier Montiglio. Personality and the emergence of the pace-of-life syndrome concept at the population level. *Philosophical Transactions of the Royal Society B: Biological Sciences*, 365(1560):4051–4063, 2010.
27. Peter A. Biro and John R. Post. Rapid depletion of genotypes with fast growth and bold personality traits from harvested fish populations. *Proceedings of the National Academy of Sciences, USA*, 105(8):2919–2922, 2008. doi: 10.1073/pnas.0708159105.
28. Jolle W Jolles, Neeltje J Boogert, Vivek H Sridhar, Iain D Couzin, and Andrea Manica. Consistent individual differences drive collective behavior and group functioning of schooling fish. *Current Biology*, 27(18):2862–2868, 2017. ISSN 0960-9822.
29. Valerio Sbragaglia, Josep Alós, Kim Fromm, Christopher T. Monk, Carlos Díaz-Gil, Silva Uusi-Heikkilä, Andrew E. Honsey, Alexander D.M. Wilson, and Robert Arlinghaus. Experimental size-selective harvesting affects behavioral types of a social fish. *Transactions of the American Fisheries Society*, 148(3):552–568, 2019. ISSN 0002-8487 1548-8659. doi: 10.1002/tafs.10160.
30. James E Herbert-Read, Emil Rosén, Alex Szorkovszky, Christos C Ioannou, Björn Rogell, Andrea Perna, Indar W Ramnarine, Alexander Kotrschal, Niclas Kolm, and Jens Krause. How predation shapes the social interaction rules of shoaling fish. *Proceedings of the Royal Society B: Biological Sciences*, 284(1861):20171126, 2017. ISSN 0962-8452.
31. Anne Elizabeth Magurran and Tony J Pitcher. Provenance, shoal size and the sociobiology of predator-evasion behaviour in minnow shoals. *Proceedings of the Royal Society B: Biological sciences*, 229(1257):439–465, 1987. ISSN 0080-4649.
32. Randal S. Olson, David B. Knoester, and Christoph Adami. Evolution of swarming behavior is shaped by how predators attack. *Artificial Life*, 22(3):299–318, 2016. doi: 10.1162/ARTL_a_00206%M27139941.
33. Manfred Milinski. Experiments on the selection by predators against spatial oddity of their prey. *Zeitschrift für Tierpsychologie*, 43(3):311–325, 1977. ISSN 0044-3573. doi: 10.1111/j.1439-0310.1977.tb00078.x.
34. Valerio Sbragaglia, Jose Fernando López-Olmeda, Elena Frigato, Cristiano Bertolucci, and Robert Arlinghaus. Fisheries-induced evolution of the circadian system and collective personality traits. *bioRxiv*, page 622043, 2019. doi: 10.1101/622043.
35. Culum Brown and Eleanor Irving. Individual personality traits influence group exploration in a feral guppy population. *Behavioral Ecology*, 25(1):95–101, 2013. ISSN 1045-2249. doi: 10.1093/beheco/art090.
36. Kolbjørn Tunstrøm, Yael Katz, Christos C. Ioannou, Cristián Huepe, Matthew J. Lutz, and Iain D. Couzin. Collective states, multistability and transitional behavior in schooling fish. *PLOS Computational Biology*, 9(2):e1002915, 2013. doi: 10.1371/journal.pcbi.1002915.
37. Richard Bainbridge. The speed of swimming of fish as related to size and to the frequency and amplitude of the tail beat. *Journal of Experimental Biology*, 35(1):109–133, 1958. ISSN 0022-0949.
38. Roy Harpaz, Gašper Tkačik, and Elad Schneidman. Discrete modes of social information processing predict individual behavior of fish in a group. *Proceedings of the National Academy of Sciences, USA*, 114(38):10149–10154, 2017. ISSN 1091-6490 0027-8424. doi: 10.1073/pnas.1703817114.
39. Nikolai W.F. Bode, Jolyon J. Faria, Daniel W. Franks, Jens Krause, and A. Jamie Wood. How perceived threat increases synchronization in collectively moving animal groups. *Proceedings of the Royal Society B: Biological Sciences*, 277(1697):3065–3070, 2010. ISSN 14712970. doi: 10.1098/rspb.2010.0855.
40. V. Sbragaglia, C. Gliese, D. Bierbach, A. E. Honsey, S. Uusi-Heikkila, and R. Arlinghaus. Size-selective harvesting fosters adaptations in mating behaviour and reproductive allocation, affecting sexual selection in fish. *Journal of Animal Ecology*, 88(9):1343–1354, 2019. ISSN 0021-8790. doi: 10.1111/1365-2656.13032.
41. Silva Uusi-Heikkilä, Kai Lindström, Noora Parre, Robert Arlinghaus, Josep Alós, and Anna Kuparinen. Altered trait variability in response to size-selective mortality. *Biology Letters*, 12(9):20160584, 2016. doi: 10.1098/rsbl.2016.0584.
42. S. Uusi-Heikkilä, T. Savilammi, E. Leder, R. Arlinghaus, and C. R. Primmer. Rapid, broad-scale gene expression evolution in experimentally harvested fish populations. *Molecular Ecology*, 26(15):3954–3967, 2017. ISSN 1365-294X (Electronic) 0962-1083 (Linking). doi: 10.1111/mec.14179.
43. Josep Alós, Miquel Palmer, and Robert Arlinghaus. Consistent selection towards low activity phenotypes when catchability depends on encounters among human predators and fish. *PLOS ONE*, 7(10):e48030, 2012. doi: 10.1371/journal.pone.0048030.
44. Valerio Sbragaglia, Lorenzo Morroni, Lorenzo Bramanti, Boris Weitzmann, Robert Arlinghaus, and Ernesto Azzurro. Spearfishing modulates flight initiation distance of fishes: the effects of protection, individual size, and bearing a speargun. *ICES Journal of Marine Science*, 75(5):1779–1789, 2018. ISSN 1054-3139 1095-9289. doi: 10.1093/icesjms/fsy059.
45. R. Spence, G. Gerlach, C. Lawrence, and C. Smith. The behaviour and ecology of the zebrafish, *Danio rerio*. *Biological reviews of the Cambridge Philosophical Society*, 83(1): 13–34, 2008. ISSN 1464-7931 (Print) 0006-3231. doi: 10.1111/j.1469-185X.2007.00030.x.
46. Jonathan M Cachat, Peter R Canavello, Marco F Elegante, Brett K Bartels, Salem I Elkhayat, Peter C Hart, Anna K Tien, David H Tien, Esther Beeson, and Sopan Mohnot. *Modeling stress and anxiety in zebrafish*, pages 73–88. Springer, 2011.
47. Roy Harpaz and Elad Schneidman. Social interactions drive efficient foraging and income equality in groups of fish. *bioRxiv*, page 740886, 2019. doi: 10.1101/740886.
48. Parisa Rahmani, Fernando Peruani, and Pawel Romanczuk. Flocking in complex environments – attention trade-offs in collective information processing. *arXiv*, page 1907.11691, 2019.
49. Daniel S. Calovi, Alexandra Litchinko, Valentin Lecheval, Ugo Lopez, Alfonso Pérez Escudero, Hugues Chaté, Clément Sire, and Guy Theraulaz. Disentangling and modeling interactions in fish with burst-and-coast swimming reveal distinct alignment and attraction behaviors. *PLOS Computational Biology*, 14(1):e1005933, jan 2018. ISSN 1553-7358. doi: 10.1371/journal.pcbi.1005933.
50. Pawel Romanczuk, Iain D. Couzin, and Lutz Schimansky-Geier. Collective motion due to individual escape and pursuit response. *Physical Review Letters*, 102(1):010602, jan 2009. ISSN 0031-9007. doi: 10.1103/PhysRevLett.102.010602.
51. Tamás Vicsek, András Czirók, Eshel Ben-Jacob, Inon Cohen, and Ofer Shochet. Novel type of phase transition in a system of self-driven particles. *Physical Review Letters*, 75(6): 1226–1229, aug 1995. ISSN 0031-9007. doi: 10.1103/PhysRevLett.75.1226.
52. Jure Demšar, Charlotte K. Hemelrijk, Hanno Hildenbrandt, and Iztok Lebar Bajec. Simulating predator attacks on schools: Evolving composite tactics. *Ecological Modelling*, 304: 22–33, may 2015. ISSN 03043800. doi: 10.1016/j.ecolmodel.2015.02.018.
53. Iain D. Couzin, Jens Krause, Nigel R Franks, and Simon A. Levin. Effective leadership and decision making in animal groups on the move. *Nature*, 13(4):513–516, 2005. ISSN 14607425. doi: 10.1038/nature03236.
54. M. R. Walsh, S. B. Munch, S. Chiba, and D. O. Conover. Maladaptive changes in multiple traits caused by fishing: impediments to population recovery. *Ecology Letters*, 9(2):142–8, 2006. ISSN 1461-023x. doi: 10.1111/j.1461-0248.2005.00858.x.
55. Stephanie M. Carlson, Curry J. Cunningham, and Peter A. H. Westley. Evolutionary rescue in a changing world. *Trends in Ecology Evolution*, 29(9):521–530, 2014. ISSN 0169-5347. doi: https://doi.org/10.1016/j.tree.2014.06.005.
56. Clémentine Renneville, Alexis Millot, Simon Agostini, David Carmignac, Gersende Maugars, Sylvie Dufour, Arnaud Le Rouzic, and Eric Edeline. Anthropogenic selection along directions of most evolutionary resistance. *bioRxiv*, page 498683, 2018. doi: 10.1101/498683.
57. Serinde J. van Wijk, Martin I. Taylor, Simon Creer, Christine Dreyer, Fernanda M. Rodrigues, Indar W. Ramnarine, Cock van Oosterhout, and Gary R. Carvalho. Experimental harvesting of fish populations drives genetically based shifts in body size and maturation. *Frontiers in Ecology and the Environment*, 11(4):181–187, 2013. ISSN 1540-9309. doi: 10.1890/120229.
58. Christian Jørgensen and Rebecca E. Holt. Natural mortality: Its ecology, how it shapes fish life histories, and why it may be increased by fishing. *Journal of Sea Research*, 75:8–18, 2013. ISSN 1385-1101. doi: http://dx.doi.org/10.1016/j.seares.2012.04.003.
59. Christian Jørgensen and Oyvind Fiksen. Modelling fishing-induced adaptations and consequences for natural mortality. *Canadian Journal of Fisheries and Aquatic Sciences*, 67(7): 1086–1097, 2010. ISSN 0706-652X. doi: 10.1139/F10-049.
60. Diana M. T. Sharpe and Andrew P. Hendry. Life history change in commercially exploited fish stocks: an analysis of trends across studies. *Evolutionary Applications*, 2(3):260–275, 2009. ISSN 1752-4571. doi: 10.1111/j.1752-4571.2009.00080.x.
61. Kai Lorenzen. Allometry of natural mortality as a basis for assessing optimal release size in fish-stocking programmes. *Canadian Journal of Fisheries and Aquatic Sciences*, 57(12): 2374–2381, 2000. ISSN 0706-652X. doi: 10.1139/f00-215.
62. Jeffrey A Hutchings. Influence of growth and survival costs of reproduction on atlantic cod, *Gadus morhua*, population growth rate. *Canadian Journal of Fisheries and Aquatic Sciences*, 56(9):1612–1623, 1999. ISSN 0706-652X.
63. Douglas P. Swain, Hugues P. Benoît, Mike O. Hammill, and James A. Sulikowski. Risk of extinction of a unique skate population due to predation by a recovering marine mammal. *Ecological Applications*, 29(6):e01921, 2019.
64. S. Uusi-Heikkilä, C. Wolter, T. Meinelt, and R. Arlinghaus. Size-dependent reproductive success of wild zebrafish *Danio rerio* in the laboratory. *Journal of Fish Biology*, 77(3):552–69, 2010. ISSN 0022-1112. doi: 10.1111/j.1095-8649.2010.02698.x.
65. K. O. Darrow and W. A. Harris. Characterization and development of courtship in zebrafish, *Danio rerio*. *Zebrafish*, 1(1):40–5, 2004. ISSN 1545-8547. doi: 10.1089/154585404774101662.
66. Allan V Kalueff. *The rights and wrongs of zebrafish: Behavioral phenotyping of zebrafish*. Springer International Publishing Switzerland, 2017.
67. Alfonso Pérez-Escudero, Julián Vicente-Page, Robert C. Hinz, Sara Arganda, and Gonzalo G. de Polavieja. idtracker: tracking individuals in a group by automatic identification of unmarked animals. *Nature Methods*, 11(7):743–748, 2014. doi: 10.1038/nmeth.2994https://www.nature.com/articles/nmeth.2994#supplementary-information.
68. G. Polverino, D. Bierbach, S. S. Killen, S. Uusi-Heikkila, and R. Arlinghaus. Body length rather than routine metabolic rate and body condition correlates with activity and risk-taking in juvenile zebrafish *Danio rerio*. *Journal of Fish Biology*, 89(5):2251–2267, 2016. ISSN 0022-1112. doi: 10.1111/jfb.13100.
69. Pawel Romanczuk, Markus Bär, Werner Ebeling, Benjamin Lindner, and Lutz Schimansky-Geier. Active brownian particles. *The European Physical Journal Special Topics*, 202(1): 1–162, 2012.

DRAFT

70. Ariana Strandburg-Peshkin, Colin R. Twomey, Nikolai W F Bode, Albert B. Kao, Yael Katz, Christos C. Ioannou, Sara B. Rosenthal, Colin J. Torney, Hai Shan Wu, Simon A. Levin, and Iain D. Couzin. Visual sensory networks and effective information transfer in animal groups. *Current Biology*, 23(17):R709–R711, 2013. ISSN 09609822. doi: 10.1016/j.cub.2013.07.059.
71. Paolo Domenici. The scaling of locomotor performance in predator–prey encounters: from fish to killer whales. *Comparative Biochemistry and Physiology Part A: Molecular Integrative Physiology*, 131(1):169–182, 2001. ISSN 1095-6433. doi: https://doi.org/10.1016/S1095-6433(01)00465-2.
72. Howard C Howland. Optimal strategies for predator avoidance: the relative importance of speed and manoeuvrability. *Journal of Theoretical Biology*, 47(2):333–350, 1974. ISSN 0022-5193.
73. Laurie Landeau and John Terborgh. Oddity and the 'confusion effect'in predation. *Animal Behaviour*, 34(5):1372–1380, 1986. ISSN 0003-3472.
74. Nikolaus Hansen and Andreas Ostermeier. Adapting arbitrary normal mutation distributions in evolution strategies: The covariance matrix adaptation. *Proceedings of IEEE International Conference on Evolutionary Computation*, pages 312–317, 1996. doi: 10.1109/ICEC.1996.542381.
75. Nikolaus Hansen, Youhei Akimoto, and Petr Baudis. Cma-es/pycma on github. Zenodo, DOI:10.5281/zenodo.2559634, 2019.

DRAFT

Supporting Informations

Supplementary Note 1: Model description

The burst-coast model intends to mimic the burst-coast swimming behavior of zebrafish (*Danio Rerio*). We assume that a fish is accelerating only during the burst phase with a constant force of magnitude f_b, while no forces are present during the coast phase implying a deceleration due to friction. The differential equations of motion defining current position $\vec{r}_i$ and velocity $\vec{v}_i$ of an agent i are:

$$\frac{d\vec{r}_i}{dt} = \vec{v}_i \tag{S.1a}$$

$$\frac{d\vec{v}_i}{dt} = -\beta\vec{v}_i + \vec{F}_i(t) \tag{S.1b}$$

with $\vec{F}_i(t)$ as a finite social or environmental force vector with $|F(t)| > 0$, for fish in the bursting phase. A fish decelerates passively during the coasting phase, thus the force vector vanishes $|\vec{F}_i| = 0$. β is the friction coefficient. We consider the social or environmental force vector to determine the preferred heading direction of the fish following a burst phase. Since the burst duration was very short (see section F), the resulting heading direction of the shoaling fish might diverge from the direction of the force. After a visual check of the experimental video material, we observed the characteristic zigzag-like swimming of zebrafish. This was also evident in the trajectories of the fish (Fig. S.7) and the corresponding force parallel and perpendicular to the current velocity. The turning force often started prior to the acceleration in velocity direction and reached its maximum at the start of the burst. To account for this we split the velocity change of Eq.(S.1) into the part parallel and perpendicular to the current velocity direction $\vec{v} = v[cos(\varphi), sin(\varphi)]$ and introduce a turning parameter $\alpha > 1$ which enhance the angular change:

$$\frac{d\vec{v}}{dt} = \frac{dv}{dt}\vec{e}_r + v\vec{e}_\varphi\frac{d\varphi}{dt} \tag{S.2a}$$

$$\frac{dv_i}{dt} = -\beta v_i + \left\langle \vec{F}_i, \hat{e}_r \right\rangle \tag{S.2b}$$

$$\frac{d\varphi_i}{dt} = \frac{\alpha}{v}\left\langle \vec{F}_i, \hat{e}_\varphi \right\rangle. \tag{S.2c}$$

Note that for a point-like particle responding to an external force α must be exactly 1. The above extension was required to account in our dynamical equations of motion for the fast active turning of zebrafish prior to acceleration along the direction of motion observed in our tracking data. Furthermore, note that the v^{-1} dependence of the angular change was, next to being directly derived from Eq. (S.1), verified by the tracking data (Fig. S.2).
The burst behavior is defined by the burst rate γ, the burst time or duration of the burst t_b, and the burst force $\vec{F}_i$. In particular the burst force $\vec{F}_i$ governs whether the fish uses social or environmental cues. The fish decides at the start of a burst with a probability P_{social} if reacting socially to the other fish or, with probability $1 - P_{social}$, to environmental cues.
The resulting burst force $\vec{F}$ is

$$\vec{F} = \begin{cases} f_{soc}\hat{f}_{soc}, & \text{if } p < P_{soc} \text{ with } p \sim U(0,1) \\ f_{env}\hat{f}_{env}, & \text{otherwise} \end{cases} \tag{S.3}$$

with $f_{env} \geq f_{soc}$ based on the assumption that a shoaling fish should react to a threat stronger than to social cues, as observed in startling responses.

A. Social forces. The social force is motivated by a three zone model (23) consisting of a repulsion zone ending at a distance r_r, followed by the alignment zone ending at r_o, and the attraction zone ending at r_a. Thereby it is $r_r < r_o < r_a$. The direction of the social forces is computed by

$$\hat{f}_{i,rep} = \mathcal{N}\left(\sum_{j\in\mathbb{S}_{i,r}} -\hat{r}_{ji}\right) \tag{S.4a}$$

$$\hat{f}_{i,alg} = \mathcal{N}\left(\sum_{j\in\mathbb{S}_{i,o}} \vec{v}_{ji}\right) \tag{S.4b}$$

$$\hat{f}_{i,att} = \mathcal{N}\left(\sum_{j\in\mathbb{S}_{i,a}} \hat{r}_{ji}\right) \tag{S.4c}$$

DRAFT

with $\hat{x} = \vec{x}/|x|$ defining a unit vector, $\vec{x}_{ji} = \vec{x}_j - \vec{x}_i$ as the difference between the vectors of fish j and i, $\mathbb{S}_{i,x}$ is the set of indices of fish in zone x of fish i, and $\mathcal{N}(\vec{x}) = \hat{x}$ is a normalization operator. We assume Voronoi interactions because they provide a reasonable approximation to visual networks (70) and can be efficiently computed. Therefore the sets $\mathbb{S}_{i,x}$ with $x \in [r, o, a]$ are composed only of Voronoi neighbors of fish i. Note that the alignment force is the sum of the velocity difference vectors $\vec{v}_{ji}$. Thus the focal fish i experiences the strongest alignment with neighbours whose velocity vectors differed the most from its own.
If neighbors of fish i are occupying different zones simultaneously the following rules are applied:

- if $\mathbb{S}_r \neq \emptyset$: $\hat{f}_{soc} = \hat{f}_r$ (repulsion dominated)
- if $\mathbb{S}_r = \emptyset$ and $\mathbb{S}_o \neq \emptyset$ and $\mathbb{S}_a \neq \emptyset$: $\hat{f}_{soc} = \mathcal{N}(|\mathbb{S}_a|\hat{f}_a + |\mathbb{S}_o|\hat{f}_o)$ (weighted average)

B. Environmental force. In the absence of a predator the environmental force is modelled as a random force vector. This models the sensitivity of individual fish to environmental noise (e.g. water reflections, water perturbations, sounds), and to a resulting false-positive escape response. In the presence of a threatening agent the environmental force is modelled as a simple repulsion of the shoaling fish from the simulated predator or fishing agents

$$\hat{f}_{env} = \begin{cases} [cos(\varphi), sin(\varphi)] \text{ with } \varphi \sim U(-\Pi, \Pi) & \text{no predator present, } \mathbb{S}_{i,p} = \emptyset \\ \mathcal{N}\left(\sum_{p \in \mathbb{S}_{i,p}} -\hat{r}_{pi}\right) & \text{otherwise} \end{cases} \tag{S.5}$$

with $U(a, b)$ being a uniform distribution with a and b as lower and upper bounds, and $\mathbb{S}_{i,p}$ being the set of predator or fishing agents detected by a shoaling fish i. A predator or fishing agent is detected by a shoaling fish with probability $P_{detect} = \frac{2}{1+r_{pi}/r_f}$ which equals one at $r_{pi} = r_f$. If $P_{detect} > 1$ it is set to 1. r_f is the detection distance which was for all simulations $r_f = 7\ cm$. This value is reasonable because fish should be able to detect a predator when they are likely to be captured $r_f \geq r_{capture} = 5\ cm$ but the distance should also be close to $r_{capture}$, otherwise fish would respond too often to non-dangerous cues and because the visibility in water decays with distance. The randomness is motivated by the assumption that the shoaling fish might misinterpret reflections on the water surface as threat since there were no "real" threats in the experiment.

C. Wall-avoidance mechanism. We attempt to design the model as close to the experimental setting as possible and therefore use a circle as a boundary. The introduction of parameters describing the repulsion force from the wall was avoided by the fish following a parameter free wall-avoidance mechanism. It is based on predicting before each burst the future position $\vec{r}_{fut}$ of the shoaling fish at the next expected burst. If $\vec{r}_{fut}$ is outside of the tank, at the next burst, we compute the position at which the shoaling fish would collide with the wall. The overall force is adapted such that at the end of the coast the velocity of the shoaling fish aligns parallel to the wall. This ensures that the shoaling fish avoids the wall while pursuing its intended direction.

D. Capture probability of a single fish by a natural predator. If a shoaling fish is closer to the predator than $r_{capture}$ its probability to be successfully captured within a small time window $[t, t + \delta t]$ is

$$p_{success}(t, \delta t) = p_{confuse}(t) \cdot \gamma_a \delta t. \tag{S.6}$$

Here γ_a is the predator attack rate, and $p_{confuse}(t)$ represents the confusion effect that modulates the attack rate. The attack rate used in the simulations is $\gamma_a = 1/s$. The confusion term depends on the spatial configuration of shoaling fish around the predator and decreases $p_{success}$ the more individuals are sensed (**?**). A shoaling fish is sensed if it is closer than $r_{sense} = 4 \cdot r_{capture}$. We assume that it modulates the successful capture probability in a sigmoidal way depending on the number of sensed shoaling fish N_{sensed}:

$$p_{confuse} = 0.5 \cdot \tanh(-(N_{sensed} - N_{conf})) + 1. \tag{S.7}$$

Here $N_{conf} = 4$ is the number of sensed shoaling fish at which $p_{confuse} = 0.5$.

E. Random movement of angling agent with constant persistence length. The individual fishing agent is supposed to have a constant persistence length. It's angular change is given by

$$\frac{d\varphi}{dt} = \hat{\sigma}_\varphi \xi(t). \tag{S.8}$$

$\xi(t) \propto \mathbb{N}(0, 1)$ is Gaussian white noise with zero mean and variance of one. $\hat{\sigma} = \hat{\sigma}(v_{net})$ is the angular noise strength whose exact form and dependence is derived below.

DRAFT

Keeping the persistence length constant is equivalent with keeping the variance in angle constant after the individual fishing agent travelled a path of length = l. The time needed to travel this path-length is $t_l = l/v_f$ and the variance in angle after travelling the path is

$$Var(\varphi)(l, v_{net}) = \langle \varphi(l, v_{net})^2 \rangle \tag{S.9a}$$

$$= \langle \left(\int_0^{t_l} \hat{\sigma}_\varphi \xi(t) dt \right)^2 \rangle = \hat{\sigma}_\varphi^2 \int_0^{t_l} \int_0^{t_l} \langle \xi(t)\xi(t') \rangle dt dt' \tag{S.9b}$$

$$= \hat{\sigma}_\varphi^2 \int_0^{t_l} \int_0^{t_l} \delta_{t,t'} dt dt' = \hat{\sigma}_\varphi^2 \int_0^{t_l} dt \tag{S.9c}$$

$$= \hat{\sigma}_\varphi^2 t_l = \hat{\sigma}_\varphi^2 \frac{l}{v_{net}}. \tag{S.9d}$$

Here we used that the Gaussian white noise is uncorrelated, e.g. $\langle \xi(t)\xi(t') \rangle = \delta_{t,t'}$, with $\delta_{t,t'}$ as the Kronecker-delta. If we set $\hat{\sigma}_\varphi = \sigma_\varphi \cdot \sqrt{v_{net}}$, the variance in angle after travelling a path of length l is independent of the speed:

$$Var(\varphi)(l) = \hat{\sigma}_\varphi^2 \frac{l}{v_{net}} \tag{S.10a}$$

$$= \sigma_\varphi^2 \cdot l. \tag{S.10b}$$

F. Parameter estimation. The speed depends on the burst rate γ; therefore γ was set for each selection line according to its experimental observed value. The speed and nearest neighbor distance are emergent properties of the model and therefore were used to estimate the probability to socially update P_{soc}. The other parameters (β, f_{soc}, f_{env}, t_b) were assumed, for simplicity and suggested from experimental data, to be equal across the different selection lines. Note that the forces f_{soc} and f_{env} were not distinguishable during the experiments where we only measured the burst acceleration F. The parameters of the model are summarized in Table S.1.

The estimation of the burst acceleration F and the burst duration t_b was done by splitting all data in burst and coast phases. Burst and coast phases are characterized by an increase and decrease of the speed of the shoaling fish, respectively. t_b is the mean length and F the mean acceleration of a burst period. Their estimates for each selection line are shown in Figure S.3; considering that they did not differ significantly we used the overall mean.

The burst rate γ was computed from a Gaussian moving average over the binary time series of burst starts. Each start of a burst is represented by a 1 otherwise it was 0.

The friction coefficient was estimated from the coast phases. In Figure S.4 the mean acceleration and the minimum acceleration are plotted depending on the current speed of the shoaling fish. The linear fit indicates a slope of $-\beta = 0.082$ for the mean, and $-\beta = 0.88$ for the minimum.

The range of the different zones is hard to be estimated from experiments; therefore we first assumed that the repulsion range r_r corresponded roughly to the fish body length BL and next that $r_r \approx BL/4 \approx 0.5cm$ because the ratio of length over width was about 5.

G. Parameter optimization by covariance matrix adaptation evolution strategy. To fit the model to the data we applied the covariance matrix adaptation evolution strategy. This optimizer is a good choice if the fitness landscape is multi-modal, the search space dimension is between 5 and 100 and no gradient is known. Since we wanted to fit the measures nearest neighbour distance and speed to the experimental data, our fitness function was based on the sum of the errors standardized by their experimental standard deviation:

$$Err(\mathbb{P}, \gamma, P_{soc}) = \left(\frac{nnd - Sim(nnd; \mathbb{P}, \gamma, P_{soc})}{\sigma_{nnd}} \right)^2 + \left(\frac{v - Sim(v; \mathbb{P}, \gamma, P_{soc})}{\sigma_v} \right)^2. \tag{S.11}$$

Here nnd represents the nearest neighbour distance, v represents the average individual speed, $\mathbb{P}$ represents the set of parameter apart from γ and P_{soc} needed to run a simulation and $Sim(x; \mathbb{P}, \gamma, P_{soc})$ is the measure x computed from simulations with the latter mentioned parameters. The parameters are assumed to be the same across the different selection lines apart from the burst rate γ and the tendency to socially update P_{soc} and are listed in Table S.2. In order to not run, during optimization, in a local minimum for P_{soc} we did not optimize P_{soc} but repeated for each parameter set $\mathbb{P}$ the simulation with a different value for P_{soc}. Those values ranged from 0 to 1 and were equally spaced. For each line the smallest error, according to Eq.(S.11), of all different values for P_{soc} contributed to the total error. Therefore, the total error of using the parameter set $\mathbb{P}$ and considering all selection lines, defined by their burst rate γ, is:

DRAFT

$$E(\mathbb{P}) = \frac{1}{3}(min(Err(\mathbb{P}, \gamma_{LH}, P_{soc}), P_{soc}) + \\ min(Err(\mathbb{P}, \gamma_{RH}, P_{soc}), P_{soc}) + \\ min(Err(\mathbb{P}, \gamma_{SH}, P_{soc}), P_{soc})). \tag{S.12}$$

This allows to reduce the number of parameters (five) needed to be optimized. The disadvantage to run for each parameter set $\mathbb{P}$ a scan of all possible P_{soc} can be eased by using parallelization (here on a 40 core machine). Thus for each evaluation of Eq. (S.12) the number of parameter combinations which needs to be simulated is the number of selection lines (three), specified by the line specific burst rate, times the number of different values for P_{soc}. An illustration of a typical evaluation is shown in Figure S.1. The $\langle nnd \rangle$ and $\langle v \rangle$ were estimated from 40 samples for each parameter set with independent initial conditions.
We fixed a few parameters to values estimated (see Section F), and choose the parameters alignment range (r_o), social force (f_{soc}), environmental force (f_{env}), friction coefficient ($beta$) and turning coefficient (α) as the ones to be optimized by the covariance matrix adaptation evolution strategy. Those parameters have been chosen to be optimized because they were difficult ($\beta,\ r_o$) or impossible ($f_{soc},\ f_{env},\ \alpha$) to be estimated. We first optimized the repulsion range and the attraction range as well. However, for all optimization runs they resulted in values close to zero for r_r and values consistently above $25\ cm$ for the attraction range, which is almost half of the system size (tank radius of $R = 30\ cm$). Thus we fixed the values to speed up the process. The fixed and optimized parameters and their values are summarized in Table S.2. Next to the good ability to estimate some parameters it was unnecessary to optimize all parameters because some share the same effect. For example the burst duration, burst rate and the strength of social or environmental force had a direct impact on the speed. The burst rate was fixed because it could be well estimated from the data. However, each line had a specific value because it had a strong impact on the average speed.
The most important parameter optimized by the covariance matrix adaptation evolution strategy is the probability to consider social cues instead of environmental ones. Our optimization results indicated that: p_{soc} (large-harvested line: LH) < p_{soc} (random-harvested line: RH) < p_{soc} (small-harvested line: SH)
In order to show the generality of the optimization, we ran a five-dimensional parameter scan, computed the error according to Eq. (S.12) and checked if the simulation was, with respect to the optimization result:

- **consistent**: $p_{soc}(LH) < p_{soc}(RH) < p_{soc}(SH)$.
- **partly consistent**: $p_{soc}(LH) < p_{soc}(RH) = p_{soc}(SH)$ or $p_{soc}(LH) = p_{soc}(RH) < p_{soc}(SH)$.
- **unclear**: $p_{soc}(LH) = p_{soc}(RH) = p_{soc}(SH)$.
- **inconsistent**: $p_{soc}(LH) > p_{soc}(RH) \leq p_{soc}(SH)$ or $p_{soc}(LH) \leq p_{soc}(RH) > p_{soc}(SH)$ or $p_{soc}(LH) > p_{soc}(RH) > p_{soc}(SH)$.

Due to the high dimension the scan was very coarse, i.e. 7 points in each dimension result already in $7^5 = 16804$ different parameter configurations. A scan similar to the one in Figure S.1 was done for each of this parameter configuration which increased the number of parameter configurations to $7^5 * 3 * 26 = 1\ 310\ 946$. The average values for nearest-neighbor distance and swimming speed were obtained by averaging for each parameter configuration over 10 independent runs. In Figure S.6 the one percent of parameter configurations (≈ 169) is shown which resulted in the smallest error. From this one percent: 71 percent of the parameter configurations are consistent, 18 percent partly consistent, 0 percent unclear and 11 percent inconsistent. With these results the generality of the outcomes and the proper functioning of the covariance matrix adaptation evolution strategy algorithm was assured.

Supplementary Note 2: Alternative model for the natural predator

The model of the natural predator described in section D is kept as close as possible to the other fishing simulation scenarios. However, this implies the absence of some expected properties of a typical natural-predator scenario. Here we shown that the results in the main text remain unchanged if the expected properties are taken into account.
The simple but rather unrealistic assumptions from the model described in section D are:

- that the capture probability suddenly jumps from 0 to 1 if the prey is closer than the capture radius r_c
- that the predator can in theory attack multiple prey in the same time

Here we relax these assumptions by introducing a linear distance dependence of the capture probability $p_{capture}$ and a target selection probability.

DRAFT

The probability that a natural predator successfully captured a particular shoaling fish i within a small time window $[t, t+\delta t]$ is modelled as:

$$p_{success,i}(t,\delta t) = p_{capture,i}(t) \cdot p_{confuse}(t) \cdot p_{select,i}(t) \cdot \gamma_a \delta t \tag{S.1}$$

Here γ_a is the base predator attack rate. Whereas the time-dependent pre-factors accounted for the specific capture probability of a shoaling fish i at time t $p_{capture,i}(t)$, the probability to select shoaling fish i as target $p_{select,i}(t)$, modulated by the general predator confusion $p_{confuse}(t)$. These factors depended on the spatial configuration of the shoaling fish around the predator that was in our case solely the distance to the predator. The specific capture probability is modelled as

$$p_{capture,i} = \begin{cases} \frac{r_{capture} - r_{ip}}{r_{capture}} & \text{if } r_{ip} < r_{capture} \\ 0 & \text{otherwise.} \end{cases} \tag{S.2}$$

The predator attacks one shoaling fish at a time. The target is selected weighted by its capture probability, i.e. the predator selects the shoaling fish that is most likely to be captured if attacked,

$$p_{selected,i} = \frac{p_{capture,i}}{\sum_j p_{capture,j}}. \tag{S.3}$$

The confusion modulation is identical to the one explained in Section D.
The results produced by the model with the alternative version of the natural predator were similar to the ones reproduced in the main text (Fig. S.10). However, if the confusion effect was disabled, by setting $N_{conf} = 30$, the opposite pattern (i.e. the large harvested line was slowest exploited) was observed (see Fig. S.9).

Supplementary Note 3: Mean distance of shoaling fish to fishing agents

Here we computed the mean distance the shoaling fish kept from fishing agents. This measure is an alternative to the exploitation rate used in the main text, to quantify how well the shoaling fish avoid capture:

$$\langle d_{if} \rangle = \frac{1}{N} \sum_{i=1}^{N} \min_{f \in \mathbb{S}_f} d_{if} \tag{S.1}$$

with $d_{if} = |\vec{r}_{if}|$ as the distance between shoaling fish i and a fishing agent f. The minimum function yields the distance to the closest fishing agent. In contrast to simulations in the main text, the shoaling fish are not killed by fishing agents. Otherwise the closest fish get killed and the distance measure is corrupted. Figure S.11 and Figure S.12 show the non-standardized and standardized measure of the mean distance to the predator (F, G) and of the exploitation rate (A, D, E) respectively. The distance measured substantiated the already reported results for the exploitation rate. Note that in the natural-predator scenario (A) only the exploitation rate was estimated because the predator headed directly to the closest shoaling fish and therefore it was not possible to compare with the fishing scenarios.

Movie-S1.avi. This movie shows simulations in the circular area with parameters adjusted such that only the wall avoidance mechanism changes the path of the shoaling fish. The parameters used correspond to the estimated ones from Table S.2 but the alignment, attraction range and p_{soc}. Those parameters were set such that the agents always updated according to social information $p_{soc} = 1$, but never had any neighbors due to short ranges $r_o = r_a = 0.5cm$. Thus the agents effectively swim always straight until they come in conflict with the wall. Then the wall avoidance mechanism started.

Movie-S2.avi. Eight shoaling fish are simulated in a circular area with fitted social interaction. The parameters used correspond to the estimated ones from Tab.(S.2) with $p_{soc} = 0.85$.

Movie-S3.avi. Thirty agents simulated in a rectangle of length $L = 100cm$ with periodic boundary conditions in the predator scenario. The parameters used correspond to the estimated ones from Tab.(S.2) with $p_{soc} = 0.77$. Note that the predator, in red, moves with a speed of $v_p = 22.5cm/s$ and therefore faster as the average velocity of shoaling fish. However, it moves directly to the closest prey and therefore covers the prey until it get killed. Due to the confusion effect the killing probability was lowered and it happens that the predator stays for a notable time above the targeted fish.

Movie-S4.avi. Thirty agents simulated in a rectangle of length $L = 100cm$ with periodic boundary conditions in the angler scenario. The parameters used correspond to the estimated ones from table S.2 with $p_{soc} = 0.77$.

Movie-S5.avi. Thirty agents simulated in a rectangle of length $L = 100cm$ with periodic boundary conditions in the trawling scenario. The parameters used correspond to the estimated ones from table S.2 with $p_{soc} = 0.77$.

DRAFT

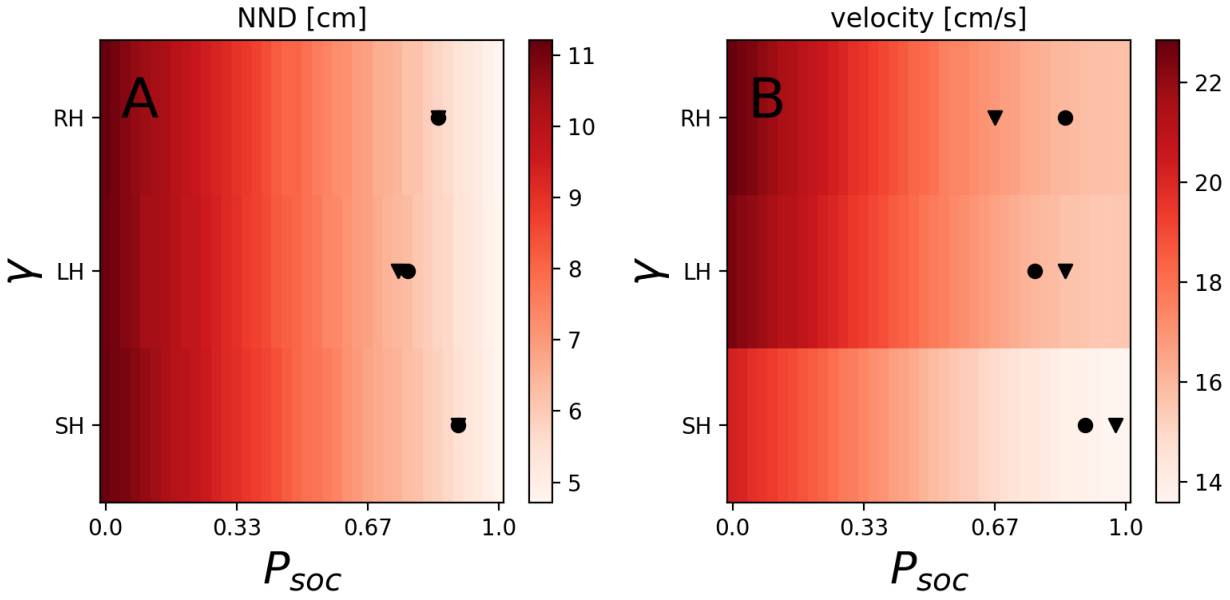

Fig. S.1. Simulations with varying social update probability (P_{soc}) for the different harvesting lines, defined by their specific burst rate γ. Solid circles represent the P_{soc} for each selection line used to compute the smallest error Eq. (S.12). The triangles represent the best fit to experimental data for (A) the nearest neighbor distance and (B) the speed v. The resolution for P_{soc} was 0.025. The burst rates γ for the different selection lines were $\gamma_{LH} = 3.45$, $\gamma_{RH} = 3.51$ and $\gamma_{RH} = 2.91$. Each average value was computed from 40 samples. The selection lines are indicated by the following abbreviations (LH: large-harvested; RH: random-harvested; SH: small-harvested).

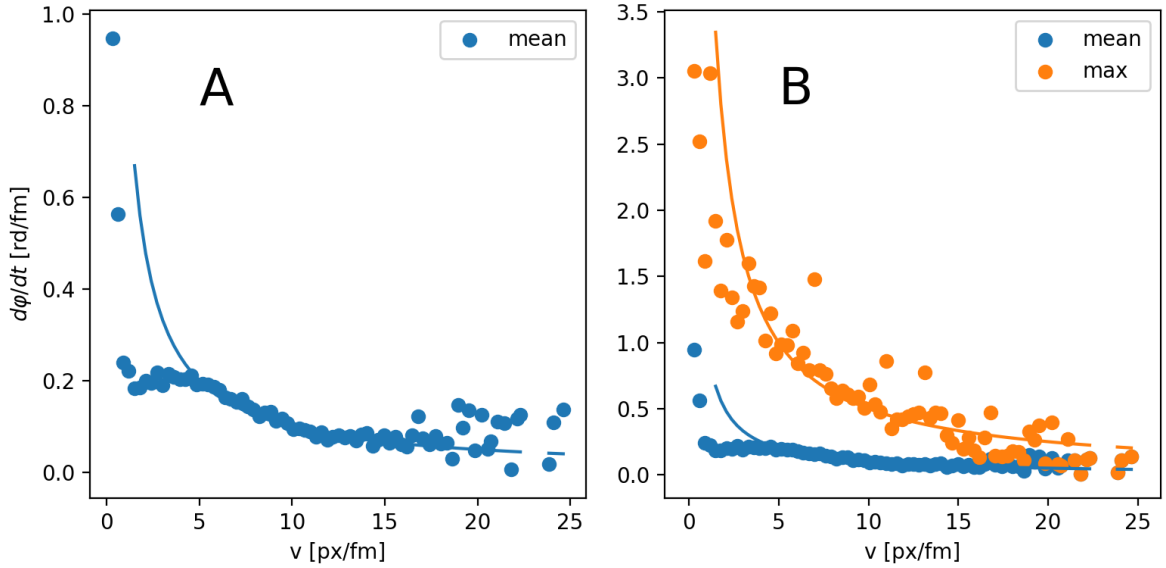

Fig. S.2. Angular change $d\varphi/dt$ depending on the velocity v. The blue dots (A, B) represent the mean values while orange dots (B) show the maximum observed value for the binned data. The blue line was $f(v) = 1/v$ and the orange line was $f(v) = 5/v$ and therefore the data agreed well with Eq. (S.2c).

model parameter	**symbol**	**estimated value/range**	**unit**
repulsion range	r_r	$\langle BL \rangle /4 \approx 0.5$	cm
alignment range	r_o	$\in [0,30]$	cm
attraction range	r_a	≈ 30	cm
friction coefficient	β	$\langle \beta \rangle = 0.082,\ max(\beta) = 0.88$	$1/s$
burst acceleration	F	62.7	cm/s^2
burst duration	t_b	0.12	s
burst rate	γ	$LH: 3.45 \pm 0.4,\ RH: 3.51 \pm 0.4,\ SH: 2.96 \pm 0.4$	$1/s$
no model parameter	**symbol**	**estimated value/range**	**unit**
speed	v	$LH: 15.8 \pm 3.0,\ RH: 16.9 \pm 2.5,\ SH: 13.1 \pm 2.5$	cm/s
nearest neighbor dist.	nnd	$LH: 6.4 \pm 1.5,\ RH: 5.8 \pm 1.6,\ SH: 5.6 \pm 1.3$	cm

Table S.1. Upper part are parameters of the burst-coast model and their estimates from the experimental data. The lower part are non-model parameters which are used to fit the model. The selection lines are indicated by the following abbreviations (LH: large-harvested; RH: random-harvested; SH: small-harvested).

fixed parameter	**symbol**	**value from Tab.(S.1)**	**unit**
repulsion range	r_r	0.5	cm
attraction range	r_a	30	cm
burst duration	t_b	0.12	s
burst rate	γ	$LH: 3.45,\ RH: 3.51,\ SH: 2.96$	$1/s$
optimized parameter		**CMA-ES result optimizing Eq.(S.12)**	
alignment range	r_o	12.6	cm
social force	f_{soc}	61.9	cm/s^2
environmental force	f_{env}	121.7	cm/s^2
friction coefficient	β	1.14	$1/s$
turning parameter	α	11.9	1
prob. to socially update	P_{soc}	$LH: 0.77,\ RH: 0.85,\ SH: 0.9$	1

Table S.2. Upper parts shows fixed parameters estimated in section (F). The lower part shows optimized parameters by the covariance matrix adaptation evolution strategy (CMA-ES) minimizing Eq. (S.12). The selection lines are indicated by the following abbreviations (LH: large-harvested; RH: random-harvested; SH: small-harvested).

DRAFT

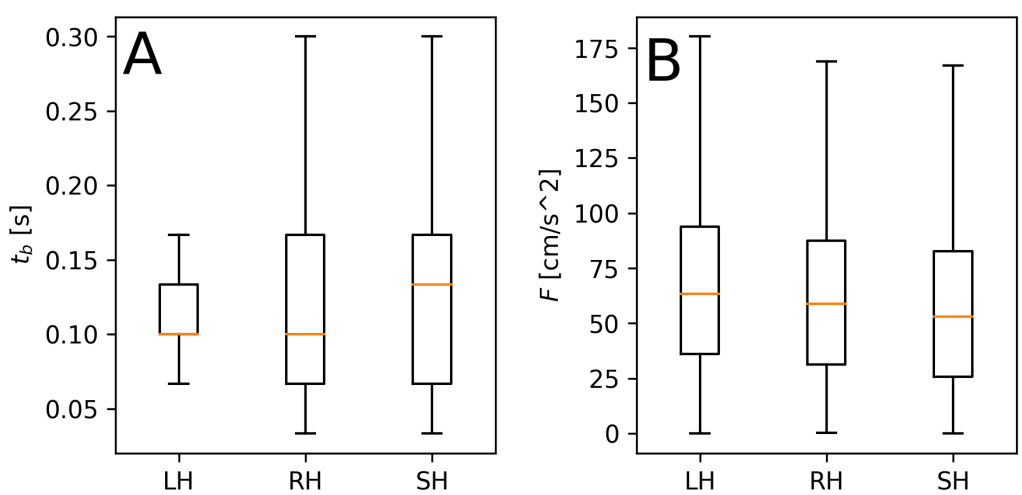

Fig. S.3. A: Burst-duration (t_b) and B: burst-acceleration (F) estimated from experimental data of the different selection lines that are indicated by the following abbreviations (LH: large-harvested; RH: random-harvested; SH: small-harvested).

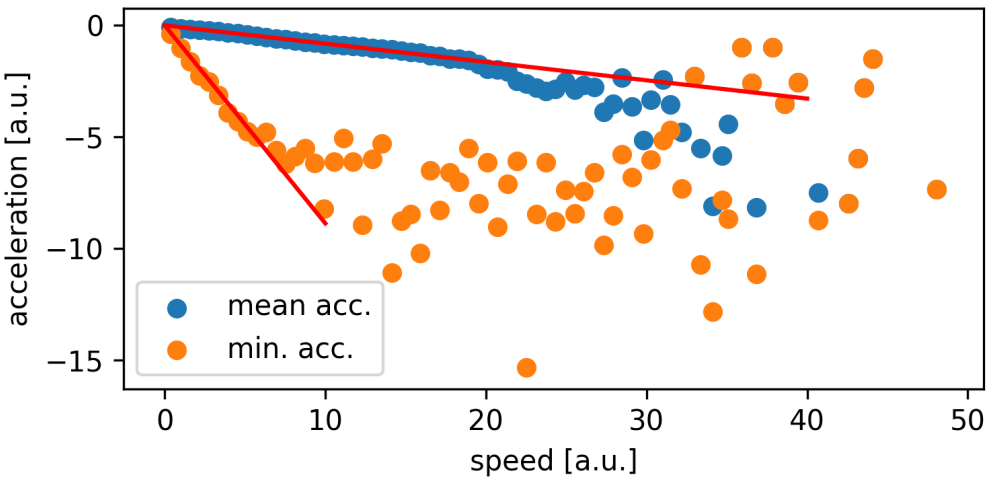

Fig. S.4. Estimation of friction coefficient from experimental data. The red lines represent linear fits of the mean and minimum acceleration for a specific velocity which results in a slope of $-beta = 0.082$ for the mean and $-beta = 0.88$ for the minimum acceleration.

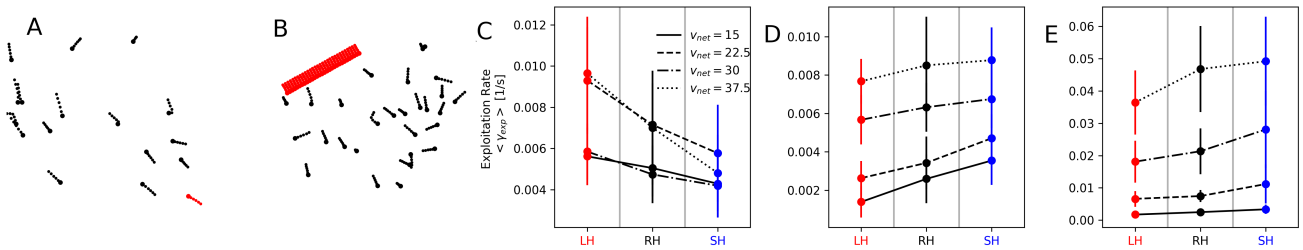

Fig. S.5. Non-standardized results of the natural-predator-like scenario (A, C), the angling-like scenario (A, D) and the trawling-like scenario (B, E) are shown. Here $N = 30$ fish swim in a box of size $L = 100cm$ with periodic boundary conditions. Compared to the shoaling fish, moving with a speed of $\langle v \rangle \approx 15cm/s$, the predator moves with $v_{net} = [15,\ 22.5,\ ,30,\ 37.5]cm/s$ while the fishing agents with $v_{net} = [0,\ 7.5,\ 15,\ 22.5]cm/s$ indicated by solid, dashed, dash-dotted and dotted line respectively. A, B show snapshots of a typical simulation; C, D, E the mean exploitation rate of the predator and fishing agents $\langle \gamma_{exp} \rangle$ and F, G the mean distance to the closest fishing agent $\langle d_{if} \rangle$. In contrast to the figure in the main-text no relative measures are shown. The selection lines are indicated by different color (red=LH: large-harvested; black=RH: random-harvested; blue=SH: small-harvested).

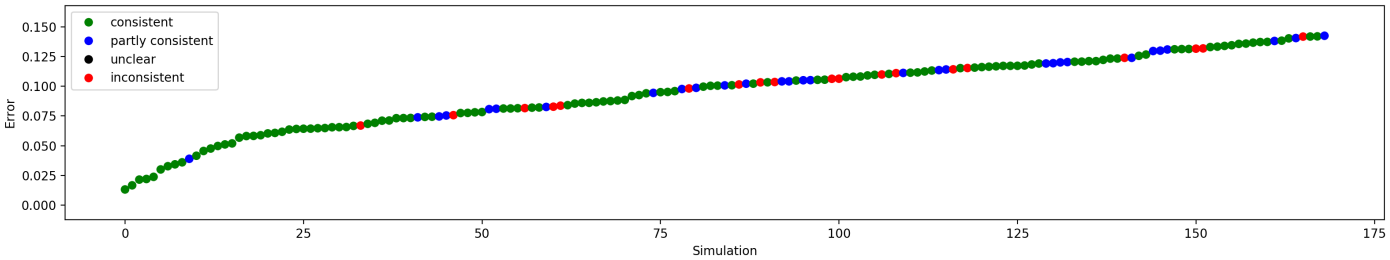

Fig. S.6. Results from five-dimensional parameter-scan used to validate the results from the Covariance Matrix Adaptation Evolutionary Strategy (CMA-ES) of the main-text. Error according to Eq. (S.12) for the one percent of the tested parameter configurations with the smallest errors. The result of the CMA-ES was that the probability to do a social burst P_{soc} differed in between the selection lines as $P_{soc}(LH) < P_{soc}(RH) < P_{soc}(SH)$. A parameter configuration was consistent if these inequalities hold, partly consistent if one of the inequalities was an equality, unclear if both inequalities were equalities and the configuration was inconsistent if one or both inequalities were opposite. The consistent, partly consistent, unclear and inconsistent cases are color coded as green, blue, black and red respectively.

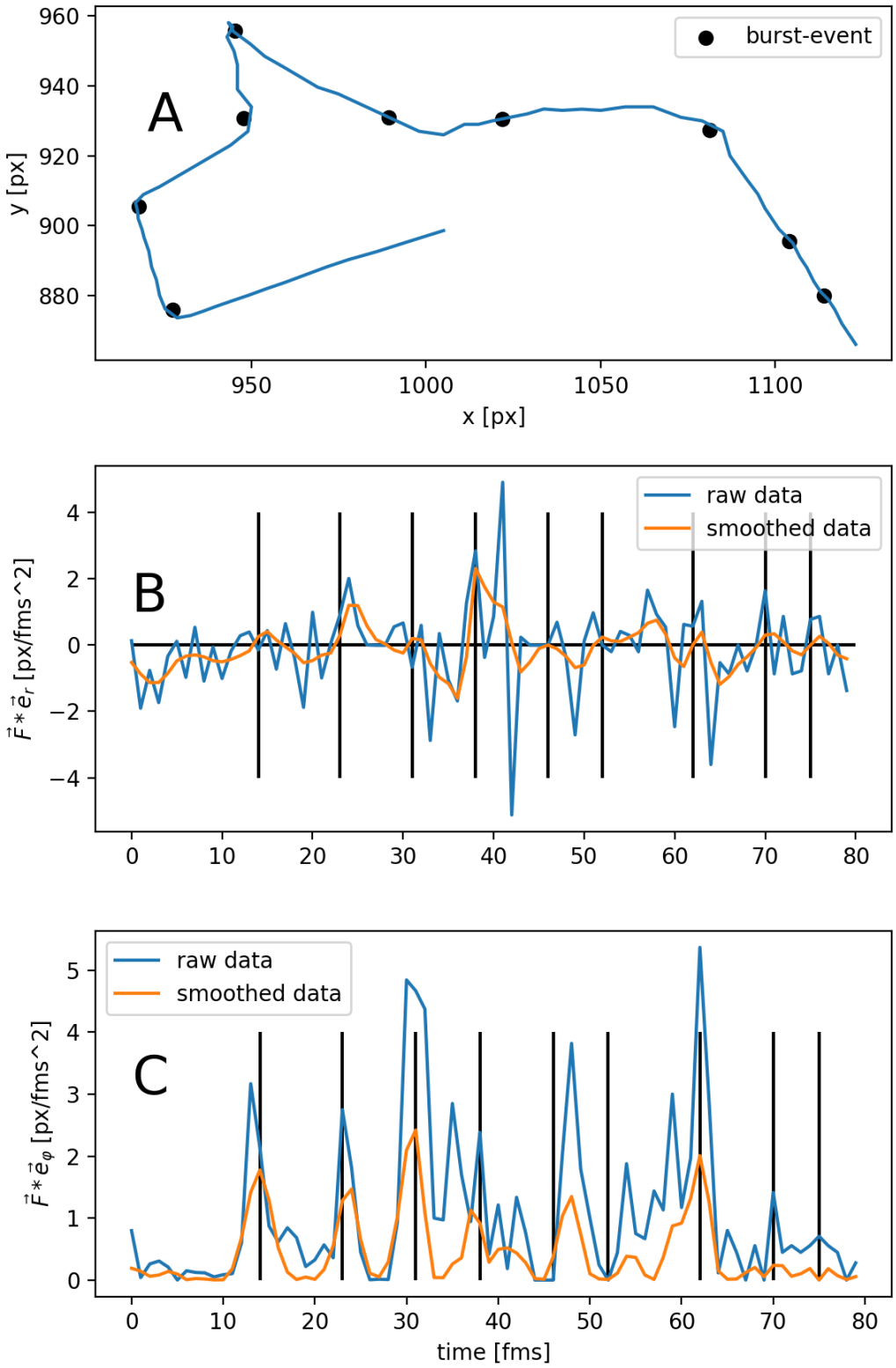

Fig. S.7. A: Part of the trajectory of a swimming zebrafish generated from raw-data of the ID-Tracker. The black dots indicate the burst events computed from the smoothed trajectory. B: Acceleration $\vec{F}$ along heading direction $\vec{e}_r$. The vertical black lines indicate burst events which are computed by the first positive acceleration of the smoothed data. C: Acceleration $\vec{F}$ perpendicular to heading direction $\vec{e}_\varphi$, i.e. direction changes. The burst events were mostly accompanied by changes in the direction.

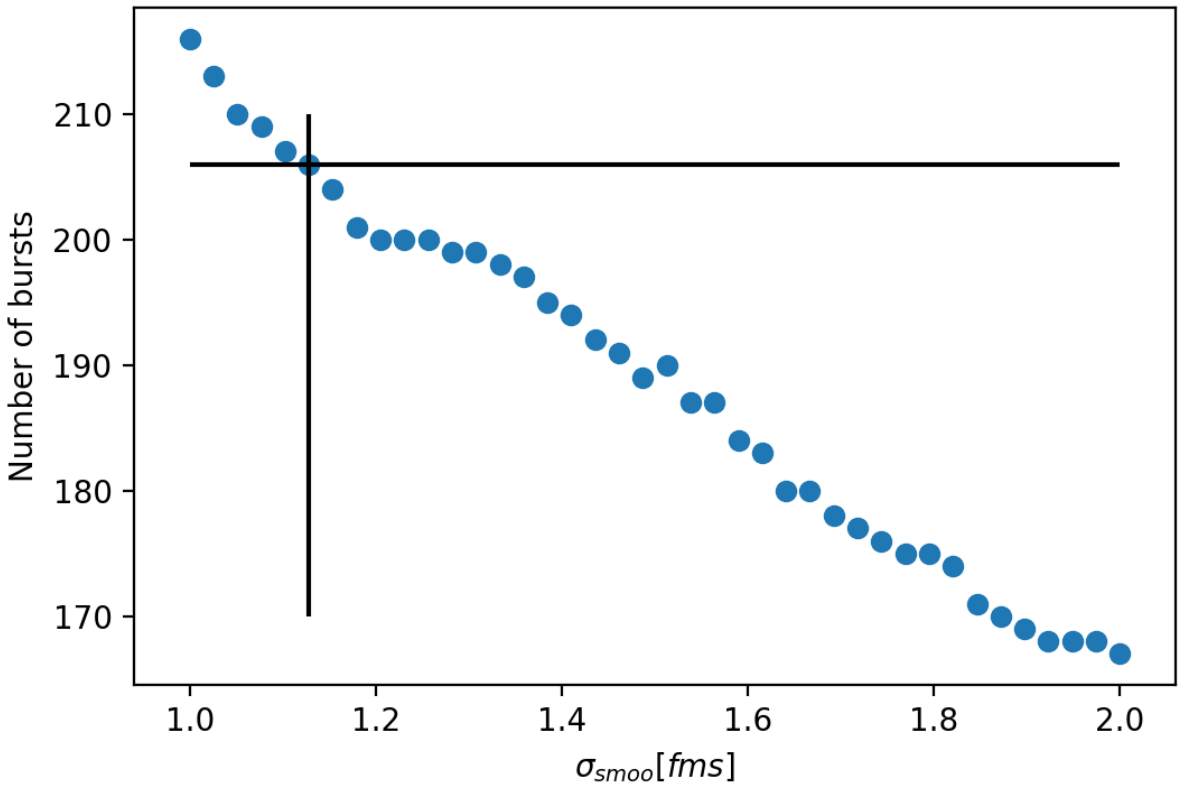

Fig. S.8. Number of burst events of a randomly selected trajectory spanning 2000 frames. The horizontal black line marks the number of manually counted burst events. Blue dots mark automatic counts of burst events on a smoothed trajectory using a moving window with a Gaussian kernel of varying standard deviation σ_{smoo}. The vertical black line indicates the standard deviation $\sigma_{smoo} = 1.13fms$ where the automatic burst detection equals the manually counted one.

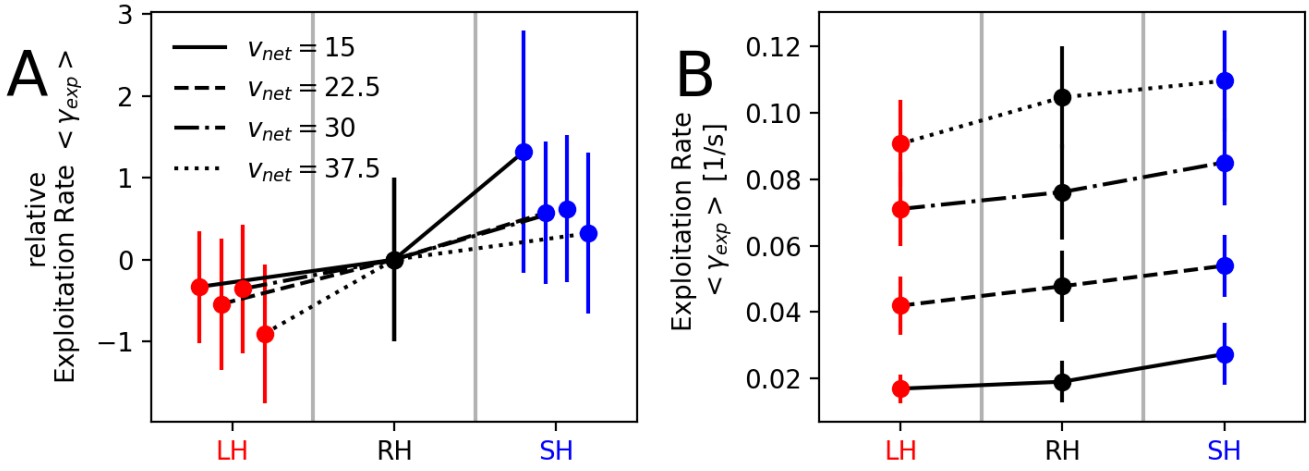

Fig. S.9. Results of the alternative predator scenario described in section 2 without confusion effect. The other parameters were identical to the predator scenario of the main text. Here $N = 30$ fish swim in a box of size $L = 100cm$ with periodic boundary conditions. Compared to the shoaling fish, moving with a speed of $\langle v \rangle \approx 15cm/s$, the predator moves with $v_{net} = [15,\ 22.5,\ ,30,\ 37.5]cm/s$ indicated by solid, dashed, dash-dotted and dotted line respectively. (A) Relative mean exploitation rate of the predator with respect to the control line (random-harvested line). The observed values are made relative to the control line by subtracting their mean and dividing by their standard deviation. The error-bars indicate the standard deviation relative to the control line. (B) the mean exploitation rate of the predator $\langle \gamma_{exp} \rangle$. The selection lines are indicated by different color (red=LH: large-harvested; black=RH: random-harvested; blue=SH: small-harvested).

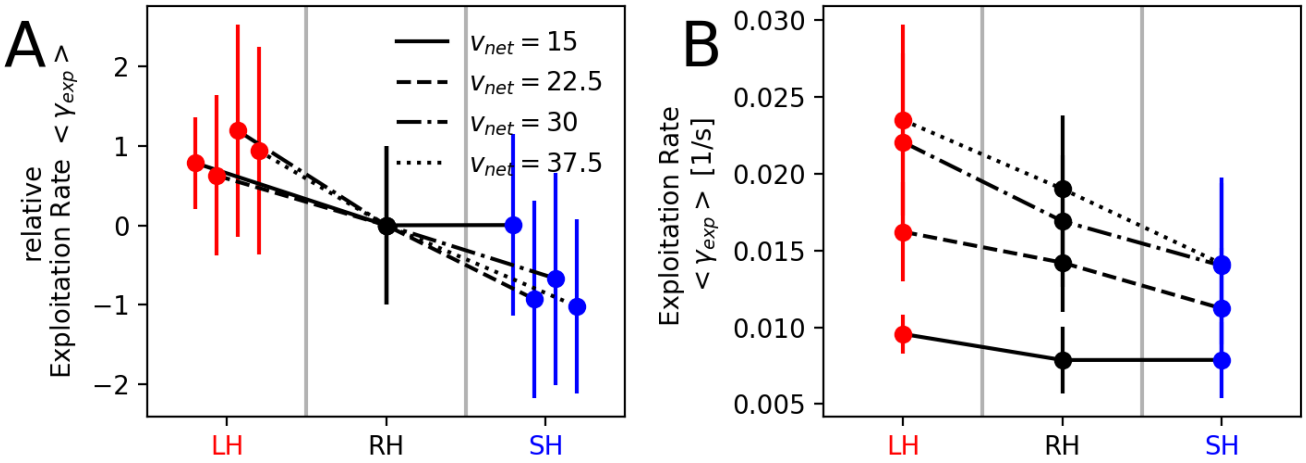

Fig. S.10. Results of the alternative predator scenario described in Sect.(2) with confusion effect. The other parameters are identical to the predator-like scenario of the main text. Here $N = 30$ fish swim in a box of size $L = 100cm$ with periodic boundary conditions. Compared to the shaoling fish, moving with a speed of $\langle v \rangle \approx 15cm/s$, the predator moves with $v_{net} = [15,\ 22.5,\ ,30,\ 37.5]cm/s$ indicated by solid, dashed, dash-dotted and dotted line respectively. (A) Relative mean exploitation rate of the predator with respect to the control line (random-harvested line). The observed values are made relative to the control line by subtracting their mean and dividing by their standard deviation. The error-bars indicate the standard deviation relative to the control line. (B) the mean exploitation rate of the predator $\langle \gamma_{exp} \rangle$. The selection lines are indicated by different color (red=LH: large-harvested; black=RH: random-harvested; blue=SH: small-harvested).

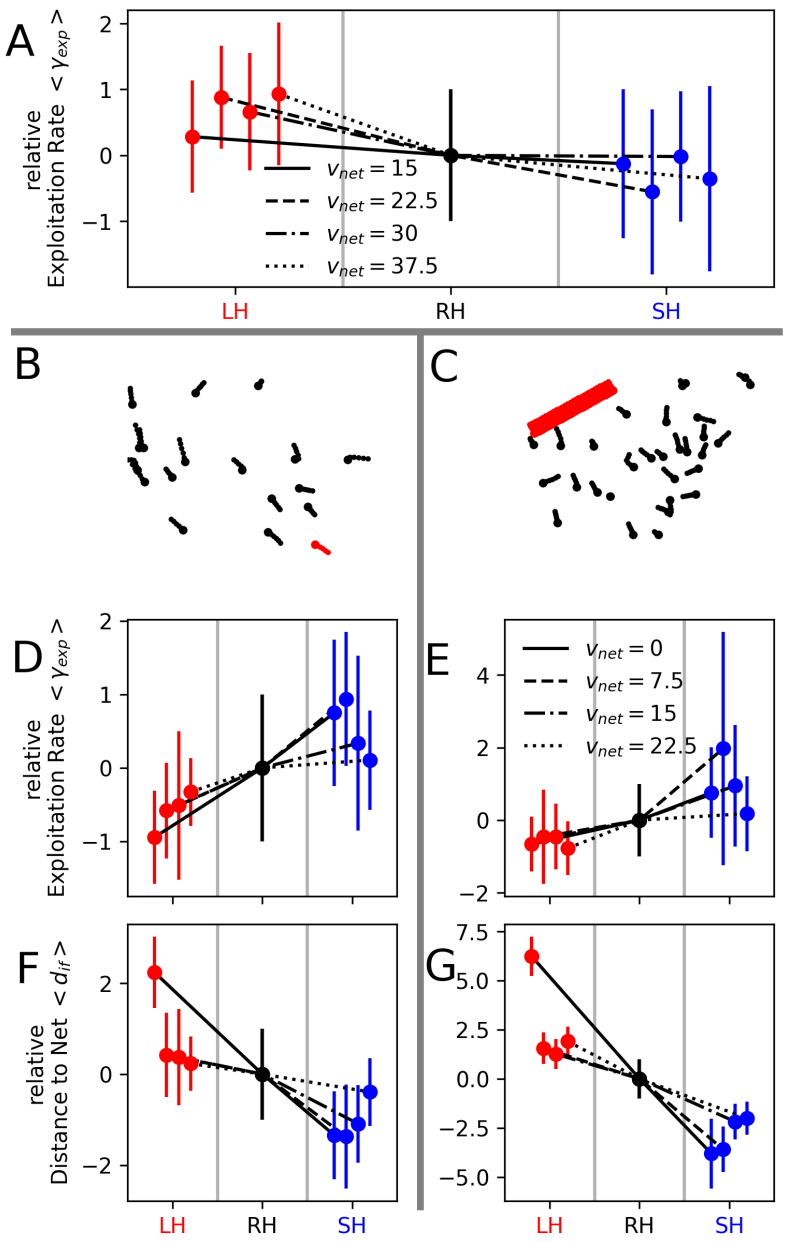

Fig. S.11. Results of the natural predator (A), the angling (B, D, F) and the trawling scenarios (C, E, G). Here $N = 30$ fish swim in a box of size $L = 100cm$ with periodic boundary conditions. Compared to the shoaling fish, moving with a speed of $\langle v \rangle \approx 15cm/s$, the predator moves with $v_{net} = [15,\ 22.5,\ ,30,\ 37.5]cm/s$ while the fishing agents with $v_{net} = [0,\ 7.5,\ 15,\ 22.5]cm/s$ indicated by solid, dashed, dash-dotted and dotted line respectively. B, C show snapshots of a typical simulation; A, D, E the relative mean exploitation rate of the predator and fishing agents $\langle \gamma_{exp} \rangle$ and F, G the relative mean distance to the closest fishing agent $\langle d_{if} \rangle$. The observed values are made relative to the control line by subtracting their mean and dividing by their standard deviation. The error-bars indicate the standard deviation relative to the control (random-harvested line) using a sample of 40 simulations. The selection lines are indicated by different color (red=LH: large-harvested; black=RH: random-harvested; blue=SH: small-harvested).

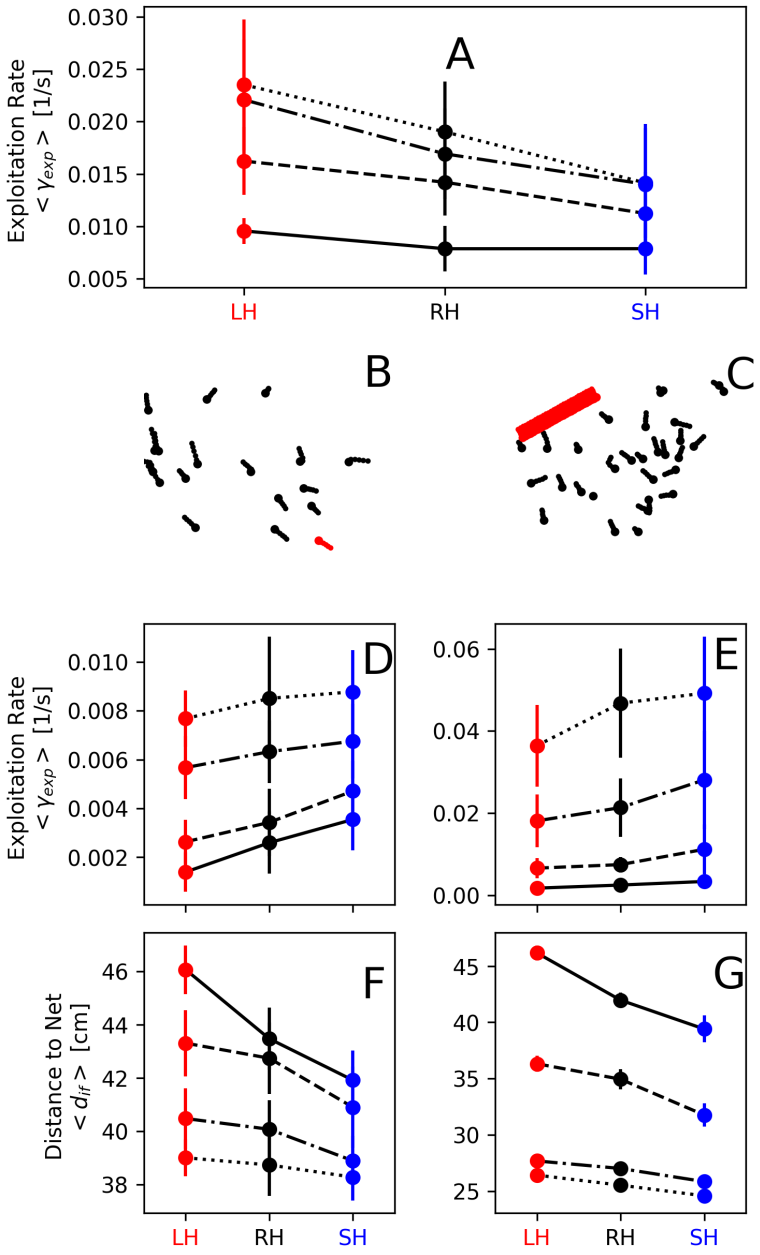

Fig. S.12. Results of the predator scenario (A), the angling scenario (B, D, F) and the trawling scenario (C, E, G) are shown. Here $N = 30$ fish swim in a box of size $L = 100cm$ with periodic boundary conditions. Compared to the shoaling fish, moving with a speed of $\langle v \rangle \approx 15cm/s$, the predator moves with $v_{net} = [15,\ 22.5,\ ,30,\ 37.5]cm/s$ while the fishing agents with $v_{net} = [0,\ 7.5,\ 15,\ 22.5]cm/s$ indicated by solid, dashed, dash-dotted and dotted line respectively. B, C show snapshots of a typical simulation; A, D, E the mean exploitation rate of the predator and fishing agents $\langle \gamma_{exp} \rangle$ and F, G the mean distance to the closest fishing agent $\langle d_{if} \rangle$. In contrast to the figure in the main-text no relative values are shown. The selection lines are indicated by different color (red=LH: large-harvested; black=RH: random-harvested; blue=SH: small-harvested).